Electrocatalysis

International Edition: DOI: 10.1002/anie.201509982
German Edition: DOI: 10.1002/ange.201509982

Carbon-Based Metal-Free Catalysts for Electrocatalysis beyond the ORR

*Chuangang Hu and Liming Dai**

Keywords:
carbon nanomaterials · hydrogen evolution · metal-free catalysts · oxygen evolution · oxygen reduction

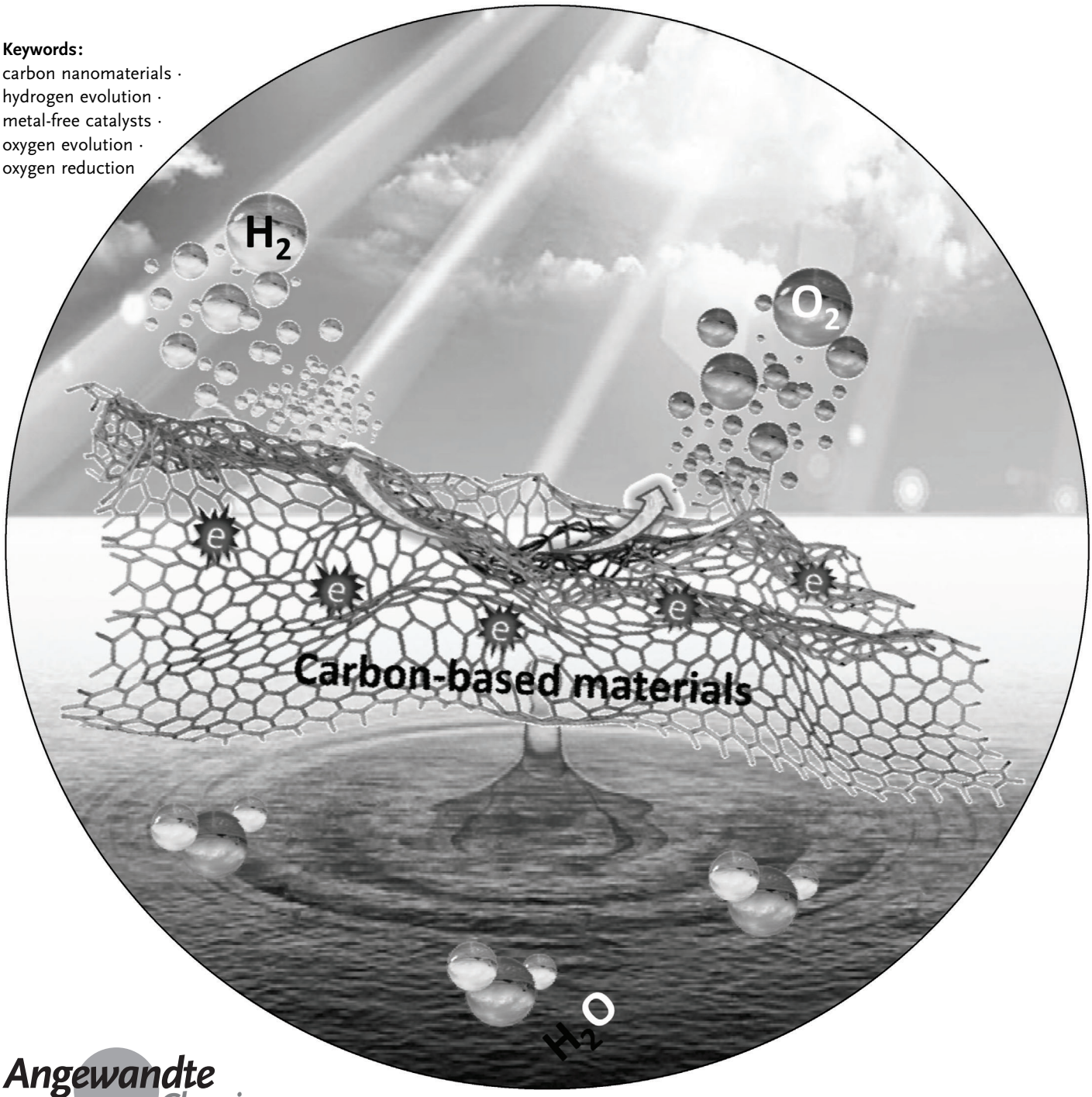

Besides their use in fuel cells for energy conversion through the oxygen reduction reaction (ORR), carbon-based metal-free catalysts have also been demonstrated to be promising alternatives to noble-metal/metal oxide catalysts for the oxygen evolution reaction (OER) in metal–air batteries for energy storage and for the splitting of water to produce hydrogen fuels through the hydrogen evolution reaction (HER). This Review focuses on recent progress in the development of carbon-based metal-free catalysts for the OER and HER, along with challenges and perspectives in the emerging field of metal-free electrocatalysis.

From the Contents

1. Introduction

Environmentally friendly and renewable energy technologies, such as fuel cells, batteries, and water splitting, hold great promise for solving current energy and environmental challenges. The three seemingly simple reactions—the oxygen reduction reaction (ORR), oxygen evolution reaction (OER), and hydrogen evolution reaction (HER)—pose great scientific challenges for the development of efficient catalysts for clean and renewable energy technologies. Noble-metal catalysts (e.g. Pt, Ir, Pd) are generally needed to promote the HER for the generation of hydrogen fuel from the electrochemical splitting of water, the ORR in fuel cells for energy conversion, and the OER in metal–air batteries for energy storage.[1] The high cost and limited reserves of noble-metal-based catalysts have precluded these renewable energy technologies from large-scale commercial applications. Therefore, considerable effort has been devoted to develop nonprecious-metal catalysts to completely or partially replace noble-metal catalysts in energy technologies. Although the amount of noble metal needed for the desired catalytic effect could be reduced by using nonprecious-metal catalysts, they are still too expensive for the commercial mass production of clean and renewable energy, or their energy conversion efficiency is too low.

Along with the intensive research efforts in developing nonprecious-metal catalysts to completely or partially replace noble-metal counterparts for clean and renewable energy technologies, a new class of carbon-based, metal-free catalysts has been discovered which could dramatically reduce the cost and increase the efficiency of fuel cells when used as alternative ORR catalysts.[2] The rational approach reported in Ref. [2] has subsequently served to nucleate a large body of studies worldwide on the research and development of metal-free catalysts for clean and renewable energy technologies. Many recent papers report carbon-based, metal-free catalysts not only for the ORR but also many other reactions, including the OER, HER, reduction of carbon dioxide for fuel generation, and reduction of triiodide to iodide in dye-sensitized solar cells for energy conversion.[3] A rapidly growing field of metal-free catalysis based on carbon nanomaterials has developed, and a substantial amount of literature has been generated. A timely review on such a rapidly growing field of great significance is highly desirable. This Review covers recent progress, critical issues, challenges, and perspectives concerning metal-free catalysts for the OER, HER, and other reactions critical to clean and renewable energy technologies.

2. Metal-Free Catalysts for the ORR

The ORR is important in many energy-conversion devices, such as fuel cells and metal–air batteries, as well as corrosion and biology.[4] Along with the rapid advances in carbon-based nanomaterials, many carbon-based metal-free catalysts have been developed that show ORR electrocatalytic activities comparable or even better than that of the Pt catalyst and with a better stability and fuel tolerance.[2,5] Since the research and development of carbon-based metal-free catalysts for ORR have been comprehensively reviewed,[6] a detailed discussion is not given herein.

3. Metal-Free Catalysts for Electrocatalysis beyond the ORR

3.1. Water-Splitting Reaction

The electrocatalytic splitting of water is an attractive reaction for the production of H_2 and O_2, as it involves no fossil fuels and no greenhouse gas emission.[7] The electrolysis reaction of water $H_2O \rightarrow 1/2O_2 + H_2$ consists of two half reactions corresponding to water oxidation and proton reduction, which take place according to the following mechanism in an acid medium:

$$\text{Anode: } 2H_2O + [C] \rightarrow [C]HO^* + H_2O + H^+ + 2e^- \rightarrow [C]O^* + H_2O + 2H^+ + 2e^- \rightarrow [C]HOO^* + 3H^+ + 3e^- \rightarrow O_2 + 4H^+ + 4e^-$$

$$\text{Cathode: } 2H^+ + [C] + 2e^- \rightarrow [C]H^* + H^+ + e^- \rightarrow H_2$$

[*] Dr. C. Hu, Prof. L. Dai
Center of Advanced Science and Engineering for Carbon (Case4-carbon), Department of Macromolecular Science and Engineering
Case Western Reserve University
10900 Euclid Avenue, Cleveland, OH 44106 (USA)

Here, [C] represents the catalyst surfaces and * represents an active reaction site on [C].

As can be seen above, hydrogen gas is evolved at the cathode, while oxygen gas is produced on the anode side during the splitting of water. The rate of hydrogen evolution is much higher than that of oxygen evolution, since hydrogen evolution can happen by direct association[8] because hydrogen interacts more weakly with [C] than oxygen. DFT calculations indicate that the direct recombination of oxygen atoms to form O_2 is impossible due to the associated large activation barrier.[9] The high overpotential of the OER means it is generally considered to be the critical bottleneck,[10] which hinders the large-scale production of hydrogen from the splitting of water.

In an alkaline electrolyte, the electrolysis of water occurs according to the following reaction mechanism:[11]

$$\begin{aligned}
\text{Cathode: } & H_2O + [C] + e^- \rightarrow [C]H^* + OH^- \\
& H_2O + [C]H^* + e^- \rightarrow H_2 + [C] + OH^- \\
& 2[C]H^* \rightarrow H_2 + 2[c] \\
\text{Anode: } & 4OH^- + [C] \rightarrow [C]OH^* + 3OH^- + e^- \\
& \rightarrow [C]O^* + H_2O + 2OH^- + 2e^- \\
& \rightarrow [C]HOO^* + H_2O + OH^- + 3e^- \\
& \rightarrow O_2 + 2H_2O + 4e^-
\end{aligned}$$

It is interesting to note that the intermediates are the same in both acidic and alkaline media. DFT calculations have been used to predict the free energy of all the intermediates in the electrochemical evolution of oxygen. The addition of an OH group to adsorbed O* to form an adsorbed HOO* was found to be a rate-limiting step. At lower potentials, water can dissociate to form adsorbed O atoms. Only after the catalyst surface is sufficiently oxidized at high potentials can water dissociation occur at a lower potential than the formation of adsorbed O*, and then the OER can start. Therefore, the oxygen adsorption energy is a good descriptor of the ability of a given surface to act as a catalyst for oxygen evolution. Specifically, one needs a material where adsorbed oxygen is destabilized relative to adsorbed HOO*.

3.2. Recent Progress on Metal-Based Catalysts for Water Splitting

Noble metals and their oxides, such as Pt, Pd, RuO_2, and IrO_2, have been regarded as the state-of-the-art catalysts for splitting water through the HER and OER. However, their scarcity, high cost, and poor long-term stability have hindered the large-scale production of hydrogen. Therefore, it is highly desirable to develop earth-abundant alternatives that have a high electrocatalytic performance.[1]

Many nonprecious-metal-based HER catalysts have been studied in the past decades with the aim of completely or partially replacing the noble metals. In particular, 3d transition metals (such as Fe, Co, and Ni), transition-metal sulfides, selenides, nitrides, carbides, phosphides, and borides as well as alloys and complexes have been demonstrated to be promising catalysts for the HER.[12–30] Recently, coordination compounds, such as a Ni bisdiphosphine based mimic of hydrogenase enzymes,[31] Cu^{II} ethylenediamine (Cu-EA), polyoxometalate (POM) based metal-organic frameworks (MOFs),[32] $[TBA]_3[\varepsilon\text{-}PMo^{V}_{8}Mo^{VI}_{4}O_{36}(OH)_4Zn_4][BTB]4/3{\cdot}x$ guest (NENU-500, BTB = benzene tribenzoate, TBA^+ = tetrabutylammoniumion), and $[TBA]_3[\varepsilon\text{-}PMo^{V}8Mo^{VI}_{4}O_{37}(OH)_3Zn_4][BPT]$ (NENU-501, BPT = [1,1′-biphenyl]-3,4′,5-tricarboxylate),[33] have also been developed as potential HER catalysts. Substantial research effort has also been devoted to the development of OER catalysts based on relatively inexpensive transition metals and their compounds, including transition-metal oxides, multimetal oxides, metal oxide based hybrids, substituted cobaltites ($M_xCo_{3-x}O_4$), hydro(oxy)oxides, phosphates, diselenide, metal oxide/diselenide hybrids, and chalcogenides.[34–49] In addition, ordered Ni_5P_4 nanoarchitectures with a "sheetlike" morphology on a Ni foil were synthesized and found to be bifunctional catalysts for both the HER and the OER.[50] However, the transition-metal-based catalysts are prone to gradual oxidation, undesirable changes in the morphology/crystalline structure, and uncontrolled agglomeration/dissolution when exposed to air or aerated electrolytes.[51] For example, the HER activity of MoS_2 in alkaline electrolytes often deteriorates in just a few cycles.[52] Most of the nonprecious-metal catalysts have a poor electronic conductivity, and hence

Liming Dai is Kent Hale Smith Professor at Case Western Reserve University in the Department of Macromolecular Science and Engineering and is also director of the Center of Advanced Science and Engineering for Carbon. He received a BSc from Zhejiang University in 1983, and a PhD from the Australian National University in 1991. After postdoctoral research at the Cavendish Laboratory in Cambridge, he spent 10 years with the Commonwealth Scientific and Industrial Research Organization in Australia. Before joining the CWRU in 2009, he was an associate professor at the University of Akron and the Wright Brothers Institute Endowed Chair Professor of Nanomaterials at the University of Dayton.

Chuangang Hu received his BS from Henan Normal University in 2011, and his PhD from Beijing Institute of Technology in 2015. He is currently a postdoctoral research associate in Professor Liming Dai's group at Case Western Reserve University. His research interests focus on carbon-based materials for energy conversion and storage.

a limited electrocatalysis performance. To overcome this limitation, conductive supports, such as graphene, reduced graphene oxide (rGO), and carbon nanotubes (CNTs) have been used to support and improve the activities of these catalysts.[53] Examples include Ni/rGO, Ni/Fe hydroxide nanoplates on CNTs, FeNi hydroxide/rGO, NiO/rGO, Co_3O_4/rGO, Co-CoO/N-rGO and Ni-NiO/N-rGO composites, metal carbides M_3C/graphene nanoribbons (M: Fe, Co, Ni), Fe@C, MoS_2-graphene/carbon nanofiber, MoS_2/N doped graphene, WS_2/CNTs, and Co@N-doped carbon catalysts.[54]

Although the use of conductive supports can improve the catalytic performance to a certain extent by enhancing the interfacial conductivity between the support and catalyst particles, the electron transfer required for water splitting on the catalytically active surface remained unchanged. Therefore, it would be ideal if carbon nanomaterials themselves, with their high conductivity, abundant active sites, and robust stability, could act as catalysts for water splitting. Indeed, nanostructured carbon materials have been developed as low-cost, metal-free catalysts for the HER and OER with good performance.

3.3. Recent Progress in Carbon-Based Metal-Free Catalysts for Water Splitting

Along with the intensive research efforts in developing transition-metal electrochemical catalysts, a new class of catalysts based on carbon nanomaterials have been developed that could dramatically reduce the cost and offer high efficiency and stability. Compared to metal-based catalysts, carbon-based metal-free counterparts have been demonstrated to show multiple advantages, including their high electronic conductivities, tunable molecular structures, abundance, and strong tolerance to acidic/alkaline environments.[55] Moreover, their metal-free nature also avoids the possible release of metal ions, and hence reduces their environmental impact. The recent availability of carbon nanomaterials, including CNTs, graphene sheets, graphite nanoplatelets, carbon nitride, and three-dimensional (3D) carbon architectures, offers new opportunities for the development of advanced metal-free catalysts with impressive catalytic performances.[56] Progress in the development of metal-free carbon-based catalysts for the OER and HER are presented in subsequent sections.

3.3.1. Recent Progress on Heteroatom-Doped Carbon Nanomaterials for the OER and HER

Doping carbon nanomaterials with heteroatoms, such as N, B, O, P, S, Cl, Se, Br, and I, has been demonstrated to be a feasible way to tune their electronic structures and (electro)chemical properties.[6,57] As the size and electron negativity of the heteroatoms are different from those of carbon atoms, the introduction of heteroatoms could cause electron modulation to change the charge distribution and electronic properties of carbon skeletons, which in turn affects their interaction with hydrogen or oxygen intermediates and ultimately their electrocatalytic activities for the OER and HER.[6,58] This, together with the doping-induced defects, could further change the chemical activity of the carbon nanomaterials, thus leading to further enhancement in the electrocatalytic activities.[6,58] In particular, heteroatom-doped carbon-based catalysts are promising for water splitting.

3.3.1.1. Nitrogen-Doped Carbon Nanomaterials

Nitrogen has an atomic size similar to that of carbon, but has a different electron configuration. Doping carbon nanomaterials with nitrogen atoms could change their electronic structures, but with a minimum disturbance to the carbon lattice. The changes in the electronic structures induced by doping of carbon nanomaterials with N atoms are attractive for a wide range of applications, including electrocatalysis.[6,59]

The doping of graphene with N atoms can induce asymmetrical charge distributions on the adjacent carbon atoms and cause larger polarizations, thereby leading to stronger affinities for H atoms.[60] Spin-unrestricted DFT calculations revealed enhanced interactions between H* and the N-doped graphene compared to those between H* and graphene. Furthermore, doping with N atoms can also alter the energy levels of the valence orbitals in the graphene matrix. This can facilitate the transfer of electrons from graphene to catalytically active sites and rapidly reduce the adsorbed H* species into molecular hydrogen.[3b] Therefore, doping with N atoms, coupled with the fabrication of a meso-/macrostructure, can be used to enhance the catalytic activities for the HER.

Doping with N atoms also has positive effects on the OER (the other half reaction of water electrolysis). For example, Yadav et al. synthesized carbon nitrogen nanotubes (CNNTs) by chemical vapor deposition (CVD; Figure 1a,b). The resultant CNNTs were found to be low-cost, efficient bifunctional catalysts for both the ORR and OER with a high activity and an excellent durability.[61] The potential at 10 mA cm^{-2}—a parameter commonly used to measure the OER activity—is smaller for CNNTs (1.68 V) than the Pt/C catalyst (1.78 V) at pH 13. The CNNTs also afford a relatively higher OER current than that of the commercial Pt/C catalyst, and is comparable to that of the IrO_2/C catalyst. Thus, doping with N atoms has significantly improved the electrocatalytic activities of the carbon-based metal-free catalysts, although the Tafel slope of the CNNTs is still large (383 mV dec^{-1}). The large difference in the Tafel slopes between the undoped CNTs (658 mV dec^{-1}) and CNNTs with different nitrogen contents suggests a large opportunity for tuning the catalytic performance by regulating the doping level. Although the exact origin of the catalytic activities are not fully understood, recent studies indicate that the insertion of N atoms in the CNTs induces active sites to facilitate the breaking of O–H bonds of water molecules and the formation of O–O bonds in oxygen molecules. Zhao et al. demonstrated that N-doped graphite nanomaterials (N/C, Figure 1c) synthesized from a N-rich polymer (melamine/formaldehyde polymer) exhibit an OER activity exceeding those of traditional electrocatalysts (e.g. IrO_2 nanoparticles) in alkaline media.[62] The optimized N/C materials show OER overpotentials as low as 1.61 V at a current density of 10 mA cm^{-2}

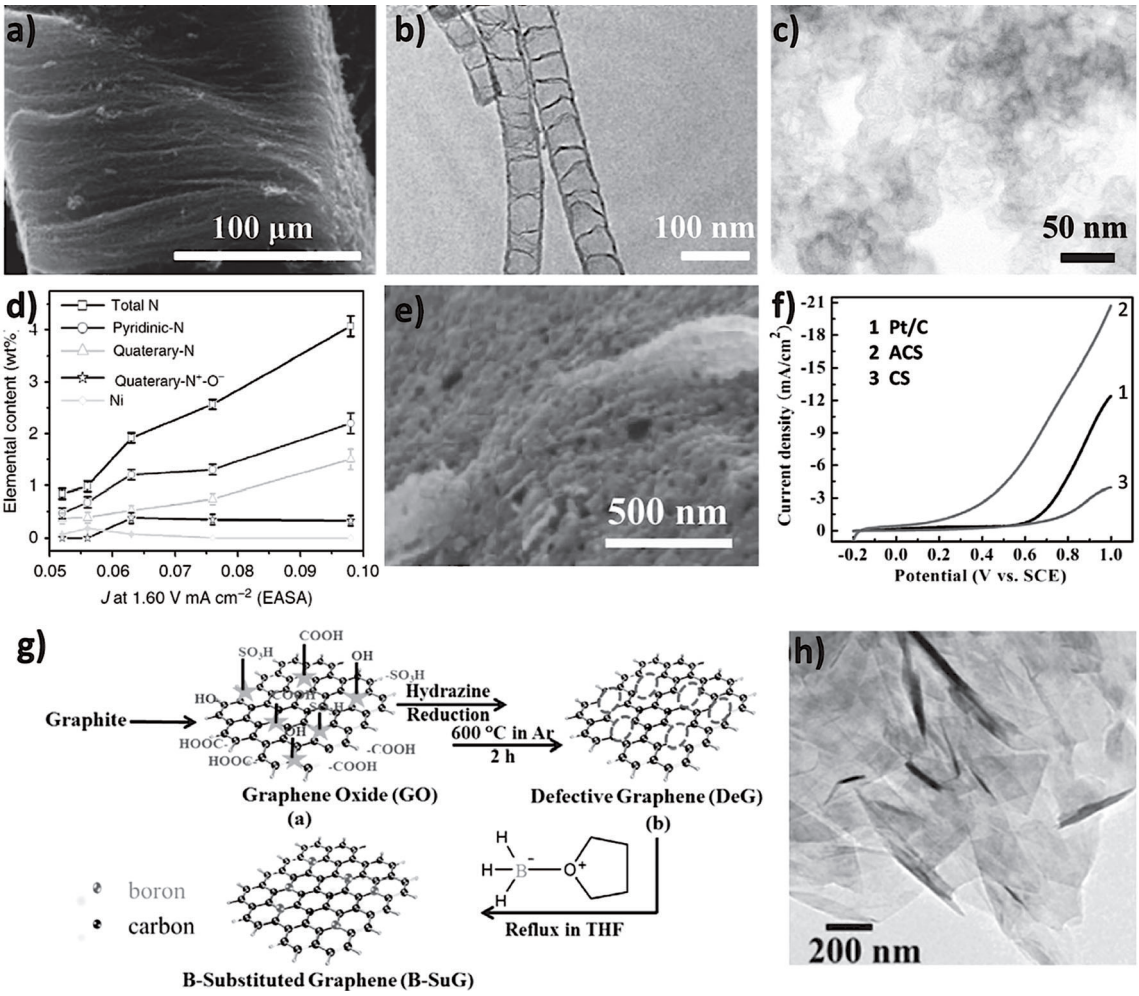

Figure 1. a,b) SEM and TEM images of CNNTs (reprinted from Ref. [61] with permission. Copyright 2015 American Chemical Society). c) TEM image of N/C materials. d) Relationship between the different elemental contents and OER activities of the N/C electrocatalysts (the potentials required to achieve 10 mA cm^{-2}; reprinted from Ref. [62] with permission. Copyright 2013 Nature Publishing Group). e) SEM image of an activated chitin-based carbon sheet (ACS). f) OER current of Pt/C, ACS, and a chitin-based carbon sheet (CS) electrode in KOH solution (0.1 mol L^{-1}) at a scan rate of 10 mV s^{-1} (reprinted from Ref. [65] with permission. Copyright 2015 Royal Society of Chemistry). g) Schematic representation of the various steps employed for the synthesis of B-substituted graphene (B-SuG). h) TEM image of B-Su (reprinted from Ref. [69] with permission. Copyright 2015 Royal Society of Chemistry).

in the absence of transition metals. The high OER activity of the N/C materials is attributed to the pyridinic-N and/or quaternary-N active sites (see Figure 1 d). Lin et al. prepared N-doped graphene (NG) by the pyrolysis of graphene oxide with polyaniline.[63] The resulting NG contains 2.4 atom % N with a high percentage of quaternary N atoms (1.2 atom %). The resultant NG also has a high catalytic activity toward the OER, and outperformed the undoped graphene, a commercial Pt/C catalyst, and a glassy carbon electrode. Another N-doped graphene catalyst with superior activity for the OER was prepared by using a hydrothermal method with ammonia as the nitrogen precursor.[64] Highly active electrocatalysts for the OER have also been made by directly converting natural chitin (the most abundant nitrogen-bearing compound in nature) into a low-cost N-doped carbon sheet through heat treatment, followed by chemical activation with $ZnCl_2$.[65] In alkaline media, the resultant activated chitin-based carbon sheets (ACS, Figure 1 e) showed a high catalytic activity for the OER, with a small overpotential of about 1.64 V (Figure 1 f).

3.3.1.2. Boron-Doped Carbon Nanomaterials

Analogous to the doping of carbon nanomaterials with N atoms, the doping of CNTs with B atoms can also enhance the graphitization[66] and reduce the resistivity at room temperature (7.4×10^{-7}–7.7×10^{-6} Ohm m versus 5.3×10^{-6}–1.9×10^{-5} Ohm m for CNTs).[67] Doping with B atoms can also shift the Fermi level of the CNTs into the valence band,[68] thereby leading to an enhanced catalytic activity for water splitting. In this context, Sathe et al. reported a facile wet-chemical synthetic method to electrocatalytically active B-substituted graphene (B-SuG) by controlled substitution of the C atoms of defective graphene (DeG) with B atoms from commercially available borane tetrahydrofuran (BH_3-THF; Figure 1 g,h).[69] The resulting B-SuG can serve as an efficient

metal-free electrocatalyst with markedly faster HER kinetics than those of its undoped counterpart. The considerably higher catalytic activity exhibited by B-SuG than DeG toward the HER can be attributed mainly to the presence of B dopants, as the doping-induced surface-defect sites and large number of surface-active (electron-rich) reduction centers can reduce the conversion barriers for the transformation of H^+ ions into H_2. In an independent study, B-doped multi-walled CNTs (B-MWCNTs) were prepared by thermally annealing MWCNTs with boric acid, and their OER activity in alkaline media (0.1 M KOH) was found to increase progressively with increasing boron content.[70]

3.3.1.3. Oxygen-Doped Carbon Nanomaterials

The doping of CNTs with O atoms can be achieved by introducing carboxy groups into the nanotube structure (surface), which, in turn, could make the nanotubes highly active and durable for the HER in acid media.[71] More specifically, the electrocatalyst consisting of O-doped CNTs showed an onset overpotential of 100 mV and required an overpotential of 220 mV to reach 10 mA cm^{-2}. The same authors used pieces of flexible and mechanically strong carbon cloth directly as a novel metal-free oxygen evolution electrode after acidic oxidation treatment for 8 h.[72] The resultant highly conductive electrode exhibited a good performance in terms of catalytic activity and stability, with an onset overpotential of 328 mV, a Tafel slope of 82 mV dec^{-1}, a 100 % Faradaic efficiency, and an overpotential of 477 mV at a current density of 10 mA cm^{-2}. These results open up new avenues to explore the design of O-doped carbon structures as electrocatalysts for water splitting.

3.3.1.4. Carbon Nanomaterials Codoped with Heteroatoms

Although N, B, and O-doped carbon nanomaterials have been demonstrated to be promising active catalysts for water splitting, their performance can be further improved by codoping with other heteroatoms (e.g. S or P), as the increased number of dopant heteroatoms and the electronic interactions between the different doped heteroatoms often generate synergistic effects.[73] Recently, graphene and other graphitic carbon materials codoped with nitrogen/sulfur and nitrogen/phosphine have been reported to show enhanced catalytic activities for both the OER and HER.

Using pyridine and thiophene as the nitrogen and sulfur precursors, respectively, Chen and co-workers synthesized N and S codoped nanoporous graphene by CVD (Figure 2a–c).[74] The optimal S and N codoped nanoporous graphene for the HER was prepared at 800 °C (denoted as NG-800). This material possessed high concentrations of dopants and geometric defects, and contained a tubular-like graphene sheet of high crystallinity (Figure 2d,e). The micrograph (inset of Figure 2e) also reveals the structure defects of the graphene lattice at the sites occupied by N and S dopant atoms. Electron energy loss spectroscopy (EELS) mapping shows the N and S atoms are homogeneously dispersed in the nanoporous graphene (Figure 2f).

The optimal NG-800 exhibited an HER onset overpotential of 130 mV and a Tafel slope of 80.5 mV dec^{-1} in an acid electrolyte. The overpotential required to deliver 10 mA cm^{-2} was 280 mV (Figure 2g), which is comparable to that of MoS_2 nanosheets, the best known Pt-free HER catalyst. DFT calculations revealed that carbon defects alone in the graphene lattice are not catalytically active for the HER, while the coupling of the S and N dopants with geometric defects in the graphene lattice produce a synergistic effect in tuning the Gibbs free energy of the H* absorption, thereby leading to the outstanding catalysis of the HER (Figure 2h). In addition, N and S self-doped carbon nanosheets have also been prepared as efficient metal-free catalysts for the HER by thermal decomposition of peanut root nodules, an abundant biological waste.[75] These N and S self-doped carbon nanosheets showed apparent electrocatalytic activity for the HER in 0.5 M H_2SO_4, with a small overpotential of only 0.027 V, a Tafel slope of 67.8 mV dec^{-1}, and good catalytic stability. DFT calculations confirmed that both S and N doping significantly changed the electronic structures of the carbon catalysts. It was found that doping with S atoms increased the electronic density on the adjacent S atoms and C atoms, while doping with N atoms only increased that on the C atoms (Figure 2i). This finding indicates that S doping, rather than N doping, played a more important role in regulating the HER activity. By using human hair, an abundant biomass material rich in elements, as the precursor, Liu et al. developed a facile and scalable method to produce N and S codoped porous carbon materials, which exhibited a high catalytic activity and stability for the HER, with an onset potential of 0.012 V, a current density of 10 mA cm^2 at 0.097 V, and a Tafel slope of 57.4 mV dec^{-1}. The observed high performance of the N and S codoped porous carbon materials for the HER could be attributed to the synergistic interactions between the N dopants and C-S-C moieties in the graphitic skeleton.[76]

As one of the elements in Group V, phosphorus (P) has the same number of valence electrons as nitrogen, but has a larger atomic size and lower electronegativity, which can introduce a defect-induced active surface for O* adsorption. Furthermore, P can induce a local charge density through its lone pair of electrons in the 3p orbital and accommodate the lone pairs of electrons from O* to initiate the OER process.[77] On the basis of the natural bond orbital (NBO) population analyses and theoretical prediction from DFT studies (Figure 3a,b), Zheng et al. explored graphene models doped or codoped with several heteroatoms (N, B, O, S, P, and/or F) and predicted that N and P codoping could afford the optimal HER activity with $|\Delta G_H| \approx 0.08$ eV.[78] To verify this prediction, the authors prepared N and P codoped graphene by annealing chemically exfoliated graphene oxide powder with a melamine and triphenylphosphine mixture at 950 °C. The final product was found to contain 4.6 atom % N and 1.63 atom % P. The incorporated N and P heteroatoms could coactivate the adjacent C atom in the graphene matrix by affecting the energy levels of its valence orbital to induce a synergistically enhanced reactivity toward the HER. The N and P codoped graphene exhibited a Tafel slope of 91 mV dec^{-1} and required an overpotential of −420 mV at

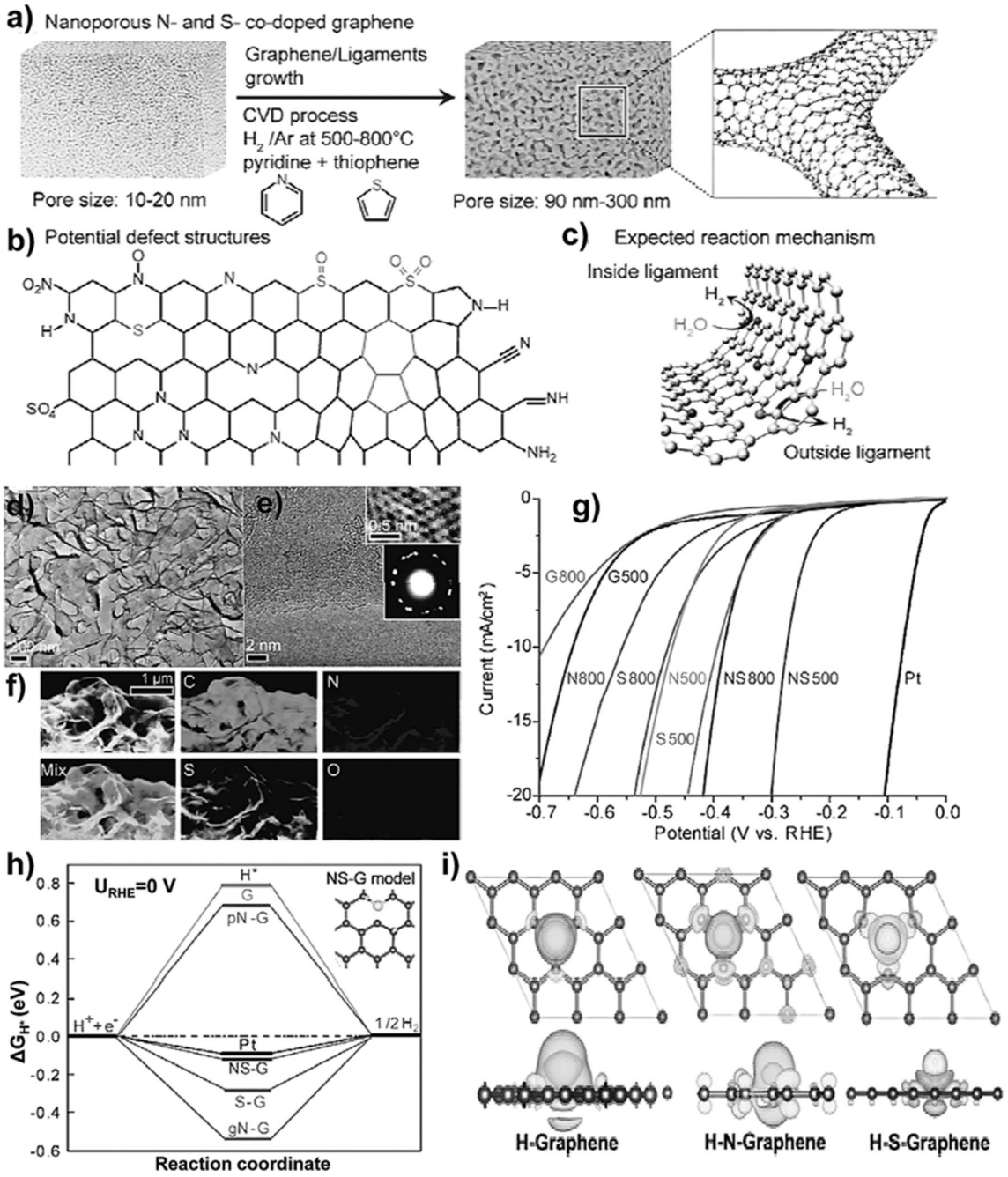

Figure 2. a–c) Illustration of the preparation of NS-G. a) Preparation of nanoporous N- and S-doped graphene by CVD. b) Potential defect structures in N- and S-doped nanoporous graphene. c) Expected reaction mechanism on the nanoporous graphene. d,e) TEM images of NS-800 at different magnifications and the corresponding selected-area electron diffraction pattern (lower right inset). The upper right inset highlights a defect structure of potential pyridinic N or S sites. f) EELs mapping of C, N, S, and O in NS-800. g) Linear-sweep voltammetry (LSV) curves of the samples produced at different CVD temperatures compared to the undoped nanoporous graphene. h) DFT-calculated HER activities of the chemically doped nanoporous graphenes with a geometric lattice defect. Shown is the calculated HER free energy diagram at an equilibrium potential for a Pt catalyst and for pyridinic (pN-G), graphitic (gN-G), sulfur-doped (S-G), and NS-G samples. The inset shows a NS-G model with a nitrogen, sulfur, and hydrogen atom (reprinted from Ref. [74] with permission. Copyright 2015 Wiley-VCH). i) Structural models and charge density of H adsorbed on the surface of graphene, N-doped graphene, and S-doped graphene (reprinted from Ref. [75] with permission. Copyright 2015 Elsevier B.V.).

10 mA cm^{-2} in 0.5 M H_2SO_4. The theoretical and experimental results clearly indicate that codoped carbon nanomaterials, similar to precious metals, could also have a great potential as highly efficient HER catalysts. Furthermore, N and P codoped multilayer nanoporous graphene has also been developed as an efficient metal-free HER electrocatalyst through a one-step solid-state reaction of urea, glucose, and phosphoric acid. This bottom-up strategy generated crumpled

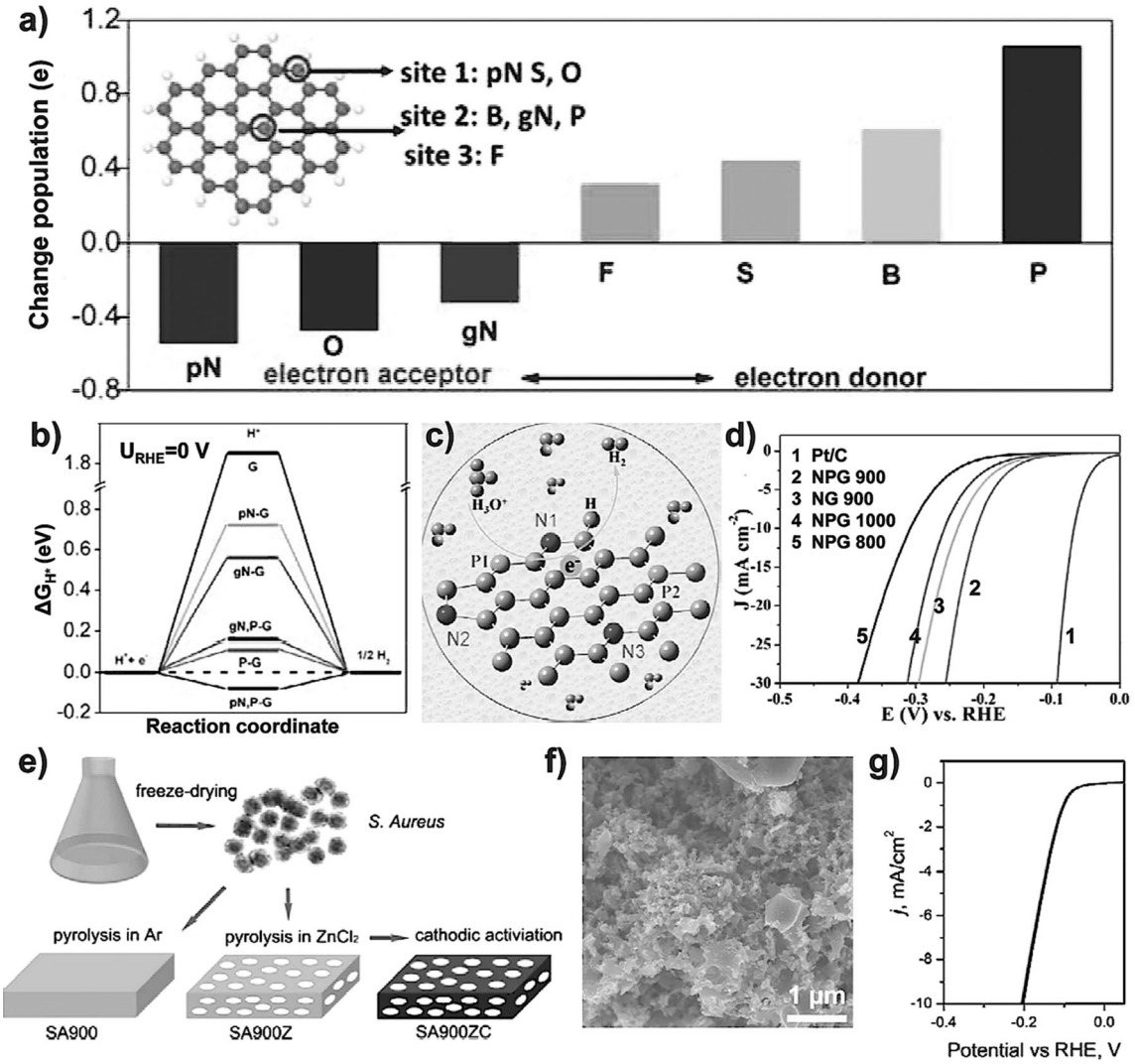

Figure 3. a) NBO population analysis of six different nonmetallic heteroatoms in a graphene matrix. pN and gN represent pyridinic and graphitic types of N, respectively. The inset shows the proposed doping sites for different elements: sites 1 and 2 are the edge and center in-plane sites, respectively, and site 3 is an out-of-plane center site in graphene. b) The calculated free energy (ΔG_{H^*}) diagram for the HER at the equilibrium potential ($U_{RHE} = 0$ V) for N- and/or P-doped graphene models (reprinted from Ref. [78] with permission. Copyright 2014 American Chemical Society). c) The structural model of highly codoped nanoporous graphene. d) Polarization curves of various samples with different sintering temperatures (reprinted from Ref. [79] with permission. Copyright 2015 Royal Society of Chemistry). e) Illustration of the synthetic procedure for the HER carbon catalyst (SA900ZC) derived from *S. aureus*. f) SEM image of SA900ZC. g) LSV curves of SA900ZC before and after 5000 cyclic voltammetry cycles (reprinted from Ref. [80] with permission. Copyright 2015 Elsevier B.V.).

and cross-linked graphene sheets with a high dopant content and well-developed porosity (Figure 3c). Subsequent annealing at 900°C (NPG900) led to a comparable onset overpotential (−0.12 V), Tafel slope (79 mV dec^{-1}), and exchange current density (0.0243 mA cm^{-2}) as some of the traditional metallic catalysts, and with an exceptional durability (Figure 3d).[79] A highly efficient HER catalyst based on carbon and with N and P dual functionalities have also been derived from a common bacterium strain (*S. aureus*; Figure 3e).[80] The obtained N and P codoped sample (SA900ZC), with a mesoporous structure generated by treatment with $ZnCl_2$ salt and cathodic activation (Figure 3f), displayed an onset overpotential as low as 76 mV, a Tafel slope of 58.4 mV dec^{-1}, and a large normalized exchange current density of 1.72×10^{-2} mA cm^{-2} as well as a high stability (Figure 3g). These values are comparable to those of the best metal-free HER catalysts.

Recently, Zhang et al. developed a template-free method for the scalable fabrication of the N and P codoped mesoporous nanocarbon (NPMC) foams simply by pyrolysis of polyaniline (PANi) aerogels synthesized in the presence of phytic acid (Figure 4a–c).[81] The resultant NPMCs have a large surface area of about 1663 m^2 g^{-1} and show bifunctional catalytic activities towards the ORR and OER in 0.1M KOH. The good catalytic activities of NPMCs for the OER were reflected by their lower onset potentials and higher currents than those of Pt/C (Figure 4d). These authors have also used a state-of-the-art OER electrode based on RuO_2 nanoparticles as a reference and found that the NPMC exhibited a lower onset potential than that of the RuO_2

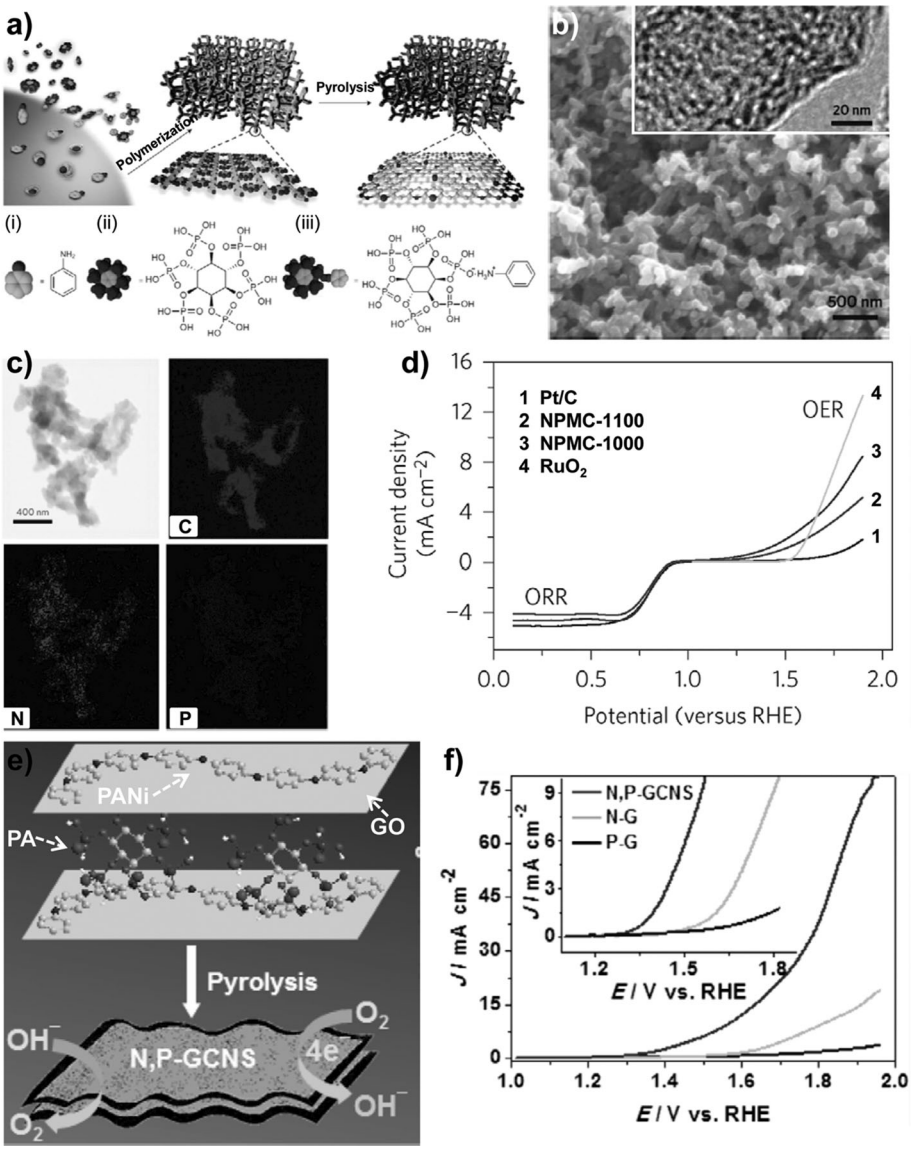

Figure 4. a) Schematic illustration of the preparation of the NPMC foams. Aniline (i) and phytic acid (ii) form a complex (iii), which undergoes oxidative polymerization into a 3D PANi hydrogel network. The PANi hydrogel is then freeze-dried and pyrolyzed in Ar to produce the NPMC. b) SEM image of NPMC-1000. Inset: the high-resolution TEM image. c) TEM image and corresponding element mapping images of NPMC-1000. d) LSV curves of NPMC-1000, NPMC-1100, RuO_2, and the commercial Pt/C catalyst on an RDE in 0.1 M KOH solution, showing the electrocatalytic activities for both the ORR and OER (reprinted from Ref. [81] with permission. Copyright 2015 Nature Publishing Group). e) Schematic illustration of the fabrication process and structure of the N- and P-doped bifunctional GCNS oxygen electrocatalyst. f) Comparison of the OER activity of various catalysts in 0.1 M KOH solution evaluated by LSV tests. Inset: Magnified view (reprinted from Ref. [82] with permission. Copyright 2015 American Chemical Society).

nanoparticles, although with slightly lower current densities at higher potentials. More recently, Li et al. fabricated N and P codoped graphene/carbon nanosheets (N,P-GCNS) by pyrolysis of a dried hydrogel composed of graphene oxide (GO), PANi, and phytic acid (PA, Figure 4e). The GO nanosheets were employed as the precursor of the graphene and the structure-directing agents for conformal coating of PANi and PA molecules during polymerization of the aniline monomers. The as-prepared N,P-GCNS can be used as a bifunctional electrocatalyst for a reversibly catalyzed OER with much better catalytic performance than the corresponding single-heteroatom-doped counterparts (Figure 4f) and even most of the reported metal-based electrocatalysts.[82] Thus, (co)doping is a powerful approach for the design and development of carbon-based metal-free catalysts for water splitting.

3.4. Combined Effects of Doping and Structure

As can be seen from the above discussion, the incorporation of heteroatom(s) into the carbon frameworks can effectively modulate the electronic structures of the surrounding carbon atoms and tune the local charge density distribution, and thereby lead to an improvement in the chemical reactivity and catalytic activity. On the other hand, the catalytic activity of a catalyst is significantly affected by the density of the active sites exposed to electrolytes. Along with the heteroatom doping, therefore, improving the exposure of active sites by tailoring the micro/macrostructures of carbon nanomaterials is also an effective way to achieve an enhancement in the catalytic performance for water splitting. This coupled with controlled heteroatom doping could also create synergistic effects.

3.4.1. The Effect of Size, Microstructure, and Dopant Location

The structure of metal-free carbon-based catalysts has a great impact on their catalytic performance. For example, Cheng et al. demonstrated that the electrocatalytic activities of pristine CNTs for the OER of water electrolysis in alkaline solutions showed a distinctive volcano-dependence on the size and/or the number of walls in the CNTs.[83] As shown in Figure 5a,b, CNTs with 2–4 walls and outer diameters of around 2–5 nm have excellent activity, fast kinetics, and a much lower energy barrier for the OER compared to single-walled CNTs (SWCNTs) and MWCNTs (CNTs with 6/7 walls). Specifically, the current density measured for the OER on the triple-walled CNTs at 1.8 V is 56 mA cm^{-2}, which is approximately

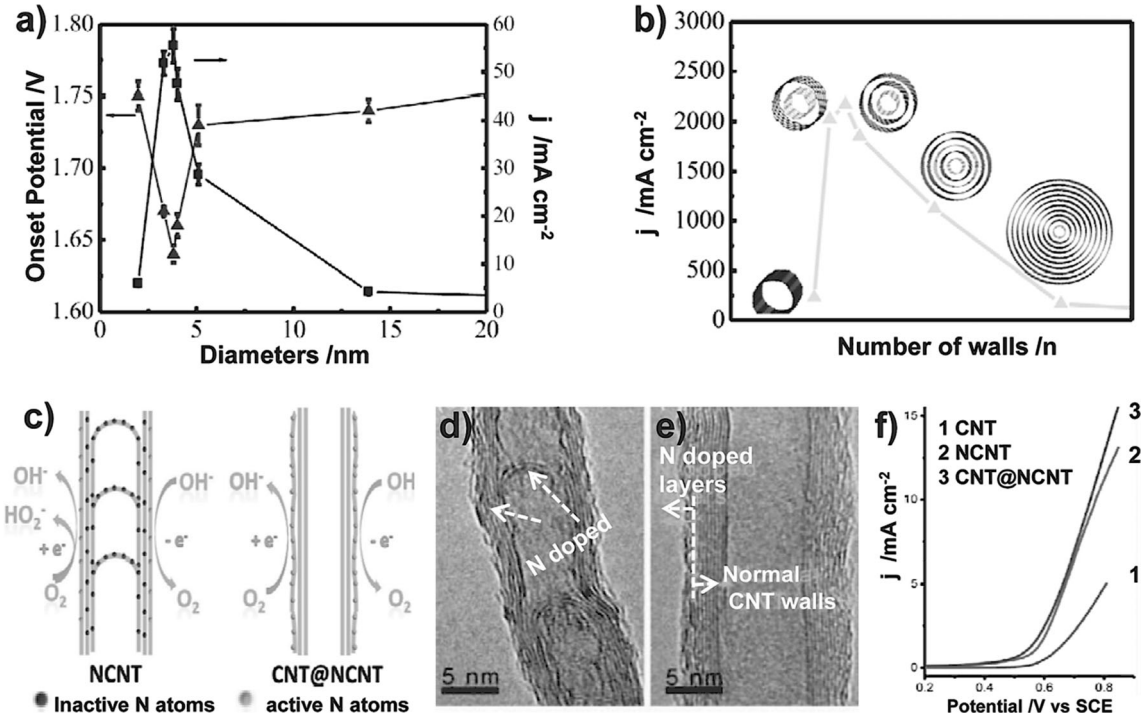

Figure 5. a) Plots of current density measured at 1.8 V and onset potential as a function of the outer diameter of the CNTs. b) Plots of the activity of CNTs for the OER in 1 M KOH solutions as a function of the number of walls. The mass-specific activity was measured at 1.8 V at a scan rate of 1 $mV s^{-1}$ and a rotating rate of 2000 rpm (reprinted from Ref. [83] with permission. Copyright 2015 Elsevier B.V.). c) Principle of the full exposure of "active sites" on the surface: NCNTs with a bulk doping of N atoms, as well as CNT@NCNT coaxial nanocables with surface-enriched nitrogen doping. TEM images of d) NCNTs, e) coaxial CNT@NCNT nanocables. f) OER currents of the CNT, NCNT, and CNT@NCNT catalysts in 0.1 M KOH solution at a scan rate of 5 $mV s^{-1}$ (reprinted from Ref. [84] with permission. Copyright 2014 Wiley-VCH).

10 times higher than on SWNTs (5.9 $mA cm^{-2}$), and 35 times higher than on MWNTs (1.6 $mA cm^{-2}$). The MWCNTs showed dual functionalities, with the outer wall providing the reaction sites for the absorption and dissociation of OH^- and OOH* species. The intact inner tubes act as the effective electronic conducting pathway for effective charge transfer through electron tunneling between the outer wall and inner tubes. The effective electron tunneling between the outer wall and inner tubes of the MWCNTs diminished as the number of walls increased because of the reduced driving force on crossing the walls of the MWNTs. The dual functionality is not possible for SWCNTs, hence their relatively poor catalytic performance.

In heterogeneous catalysis, the active sites of the catalysts are expected to be exposed at the surface, which should be as accessible as possible to the reactants to achieve a high catalytic efficiency. The unexposed active sites induced by the bulk dopant atoms are not very accessible, and consequently contribute little to the catalytic activity. CNTs can be used as a platform to demonstrate the effects of the location of the doping sites or "active sites" at the carbon surface (Figure 5c).[84] The bamboo-like structure of the traditional N-doped CNTs (NCNT) enable a complex packing of graphene layers, which often hinders rapid electron transport along the graphene layers. In contrast, the novel N-doped carbon coaxial nanocables (CNT@NCNT, Figure 5d), with the pristine CNT as the core and the N-doped carbon layers as the shell are ideal metal-free catalysts (Figure 5e). This is because this core–shell structure allows the accessible and efficient utilization of the N atoms enriched on the surface, which, coupled with the intact inner walls, can lead to the much enhanced electrocatalytic activity and high electrical conductivity (3.3 $S cm^{-1}$). Consequently, the CNT@NCNT afforded a higher oxygen reduction current, low peroxide generation, as well as a lower overpotential and higher current for the OER compared with the NCNTs under the same conditions (Figure 5f).

3.4.2. *The Macrostructure Effect*

It is important to develop catalysts with the desired macrostructures to achieve a high exposure of the active sites, and hence high HER and OER activities. In a typical gas-evolving heterogeneous catalysis, porous structures with massive pore edges can promote the interfacial catalytic reaction and the subsequent gas desorption.[85] Thus, the porosity of carbon-based catalysts is another critical factor for controlling their catalytic activities, and it is highly desirable to construct highly porous macrostructures with a large surface area.

Much effort has been devoted to the construction of porous graphene assemblies to facilitate mass transfer.[86] Crumpled graphene sheets with a large number of interlayer nanopores were demonstrated to exhibit the advantages of porous structures for electrocatalysis compared to assemblies of graphene flakes. The catalytic performance of the crum-

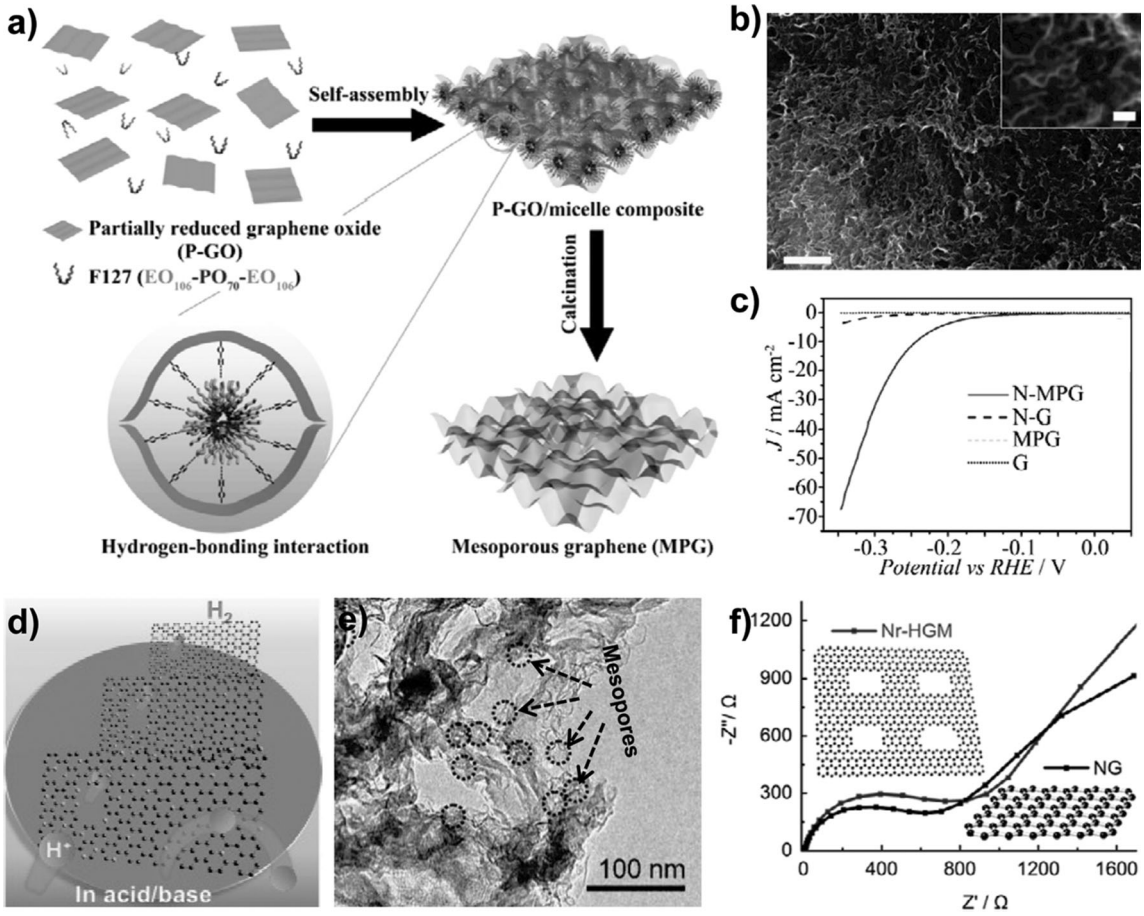

Figure 6. a) Schematic illustration of the preparation of mesoporous graphene by self-assembly of partially reduced GO and F127 micelles, followed by calcination to obtain MPG. b) SEM image of MPG. c) Polarization curves of N-MPG, N-doped pristine graphene (N-G), and pristine graphene (G) electrodes in 0.5 M H_2SO_4 at a scan rate of 5 mV s^{-1} (reprinted from Ref. [60] with permission. Copyright 2014 Nature Publishing Group). d) Schematic diagram of the HER on Nr-HGM. e) TEM image of Nr-HGM, with mesopores marked by filled circles. f) EIS data for typical Nr-HGM and NG fabricated at 900 °C (reprinted from Ref. [87] with permission. Copyright 2015 Elsevier B.V.).

pled graphene sheets can be further enhanced significantly by generating nanoholes within the constituent graphene layers (Figure 6a). In this context, N-doped graphene with relatively uniform mesopores (MPG) has been synthesized as an effective catalyst for the HER.[60] Mesoporous graphene (Figure 6b) with a high surface area (927 m^2 g^{-1}), large pore volumes (3.29 cm^3 g^{-1}), and controllable pore sizes has also been prepared by a micelle-templated synthesis, which was followed by further N-doping to generate a high electrocatalytic efficiency for hydrogen production. The obtained overpotential of 239 mV at 10 mA cm^{-2} is one of the lowest overpotentials for metal-free HER catalysts (Figure 6c).

In a similar but independent study, Ge et al. proposed an effective approach to fabricate N-rich holey graphene monoliths (Nr-HGM) by pyrolysis of GO and ammonium sulfate.[87] The unique porous structure of the Nr-HGM opened "windows" for mass transfer of the electrolyte and/or hydrogen (Figure 6d,e). Compared to large-area nonporous graphene-based catalysts (NGs), the more-exposed edges on both sides of the holey graphene introduced much more active centers for electrocatalytic reactions. Furthermore, the porous structure could also facilitate mass transfer by enhancing interactions between the solid surfaces and water molecules, and hence lead to an improved HER activity. Electrochemical impedance spectroscopy (EIS, Figure 6f) revealed better ion transfer over Nr-HGM, with a higher slope at low frequency compared to that of the NG. The poor transfer efficiency of the reactants (e.g. H^+ ions) over the NG sheets was believed to be the main hurdle for the HER. These features were reflected by the outstanding HER activities of Nr-HGM in both acidic and basic electrolytes, which indicated the importance of an opened porous structure for excellent and stable HER activity.

3.4.3. *The Effects of Electrode Architectures*

Common catalyst electrodes for electrocatalysis are usually prepared on various substrates, including 2D glassy carbon materials and 3D metal foams.[39b,88] When electrocatalysts are prepared in a 2D planar form by coating active species onto a glassy carbon using a polymer binder, the resultant electrode suffers from a limited catalyst/electrolyte contact area and unavoidable powder agglomeration. The polymer binder often increases the series resistance,[89] may

block active sites, and inhibit diffusion, thereby leading to a reduced catalytic activity.[90] In contrast, the use of 3D-structured nickel foams with a macroporosity as high as the electrode support allows facile gas transport within the electrode. However, the durability of the 3D-structured catalyst electrode needs to be further enhanced as the catalyst layer tends to peel off from the supporting foam during evolution of a large amount of gas. This limitation can be overcome by growing the active catalytic phases directly on the current collector.[88,91]

Zhao et al. have prepared a N and O codoped graphene-CNT (NG-CNT) hydrogel film electrocatalyst by filtration-assisted layer-by-layer assembly of chemically converted graphene (CCG) and CNTs, followed by N-doping with ammonia (Figure 7a,b).[88] The individual graphene sheets in this electrocatalyst were highly separated, rather than densely packed, as a result of the strong repulsive electrostatic forces. The voids between the CCG sheets could facilitate the formation of large pores to permit facile gas transport within the electrodes. Additionally, remarkable mechanical flexibility and high electrical conductivity can be achieved by the oriented assembly of CCG sheets with strong π-π intersheet interactions (Figure 7c,d). Furthermore, free-standing, self-supported hydrogel film electrocatalysts can be obtained, and used directly as the electrode. This opens up new opportunities for optimizing their microstructures and mechanical properties for facile gas transport. The codoping of the heteroatoms N and O as well as hybridization with N-doped CNTs further enhanced the catalytic activity. These unique structure features with synergistic effects have led to a surprisingly high OER activity, which even outperformed noble- (IrO_2) and some transition-metal catalysts (Figure 7e,f).

Chen et al. have fabricated a 3D N-doped carbon film by assembling graphene and ultrathin nanosheets of graphitic C_3N_4 (gC_3N_4; denoted as G-C_3N_4, Figure 7g–i) on the frameworks of cellulous fibber (CF) papers.[92] Shalom et al. demonstrated a generic method to generate ordered g-C_3N_4 on different electrodes by using a powder coating of the cyanuric acid melamine supramolecular complex.[93] The resultant carbon nitride electrode showed activity for the HER, with an enhanced overpotential of about 100 mV and current densities of about 250 mV in alkaline and neutral media, although the current density was rather poor because of the poor conductivity and low surface area (ca. 10 $m^2 g^{-1}$) intrinsically associated with the g-C_3N_4.

To overcome the shortcomings of g-C_3N_4, Zheng et al. synthesized a metal-free catalyst by coupling g-C_3N_4 with N-doped graphene (NG; Figure 8a,b), in which the g-C_3N_4 provided highly active hydrogen adsorption sites, while the N-graphene facilitated the electron-transfer process for the proton reduction. Thus, a favorable adsorption/desorption behavior with $|\Delta G_H|$ close to zero was obtained (Figure 8c).[3b] The resultant g-C_3N_4/NG hybrid catalyst showed an overpotential shift from >700 mV for individual g-C_3N_4 to about 250 mV, a current density of 10 mA cm^{-2} at $\eta = 240$ mV, good cycling durability in 0.5 M H_2SO_4, and an overpotential and Tafel slope comparable to those of the existing well-developed nanostructured MoS_2 materials (Figure 8d). Furthermore, the g-C_3N_4@NG hybrid exhibited a higher proton reduction current and electrical conductivity than

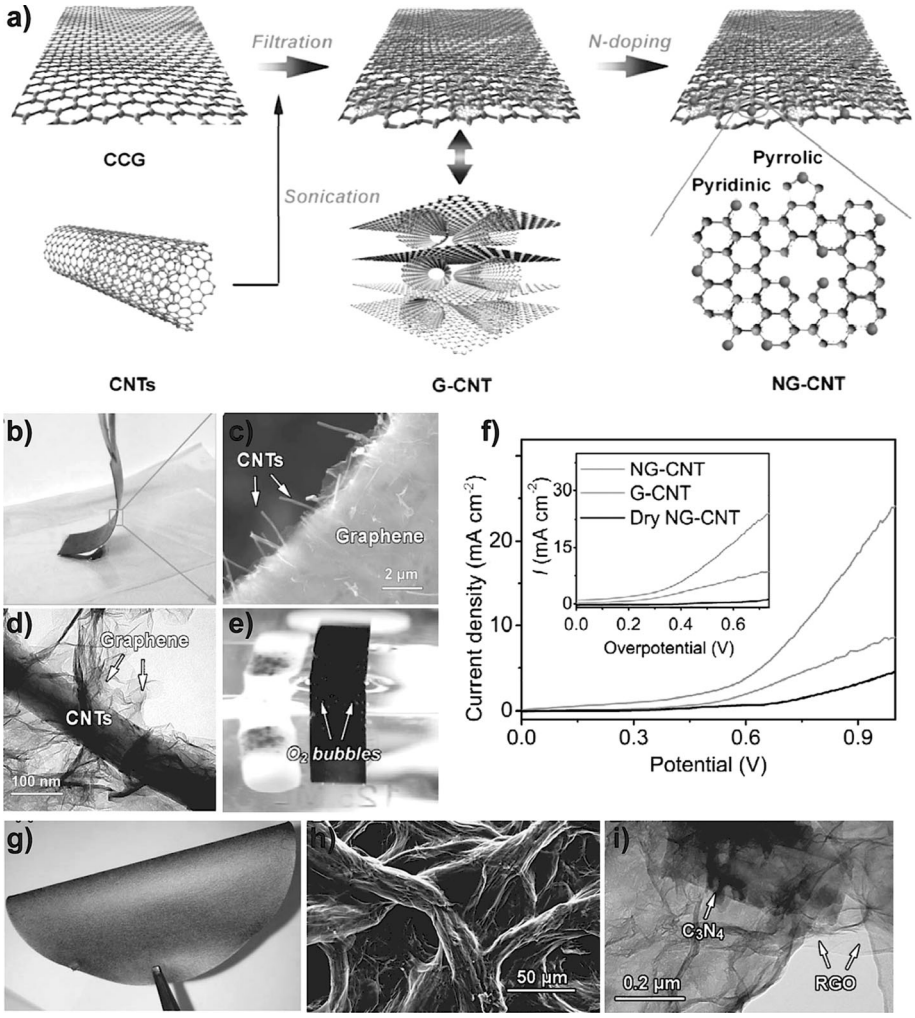

Figure 7. a) Synthetic preparation of NG-CNT. b) Optical image, c) SEM image, and d) TEM image of NG-CNT. e) Optical image of the oxygen bubbles on the catalyst electrode. f) LSV plots compared to those for G-CNT and dry NG-CNT collected at 30 mV s^{-1} in 0.1 M KOH electrolyte. Inset: the corresponding data replotted as the current density versus overpotential (reprinted from Ref. [88] with permission. Copyright 2014 Wiley-VCH). g–i) Optical microscopy, SEM, and TEM images of G-gC_3N_4 (reprinted from Ref. [92] with permission. Copyright 2015 Wiley-VCH).

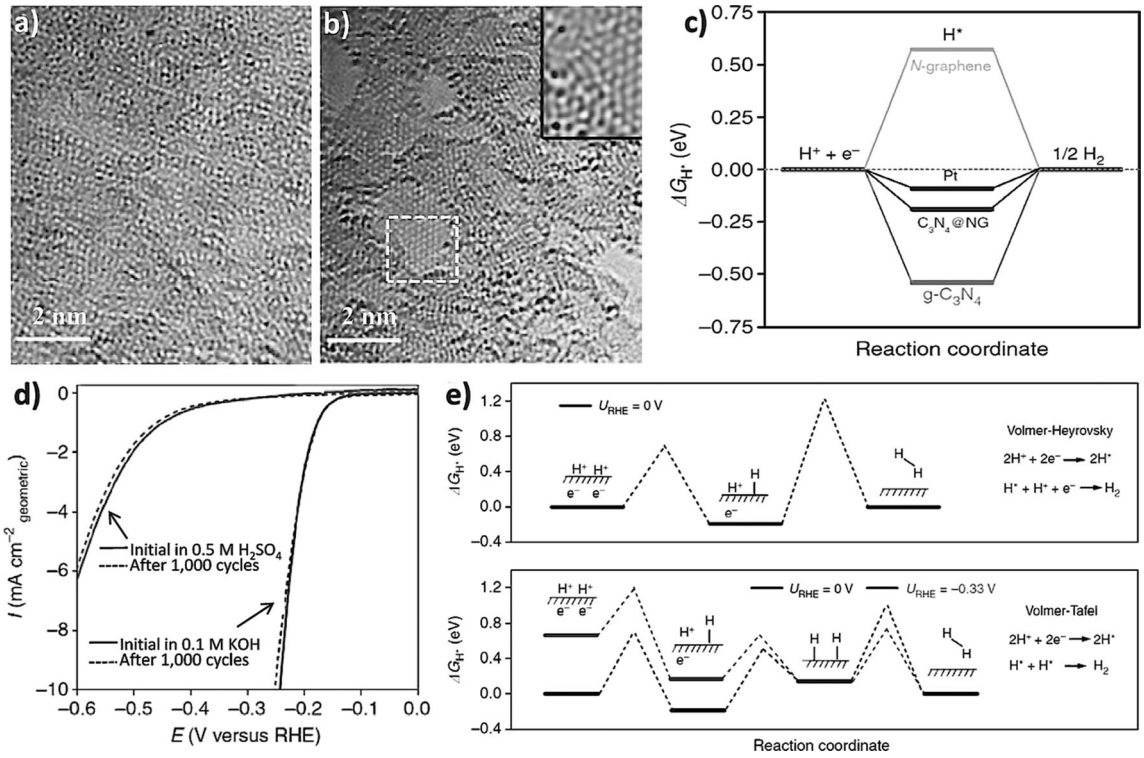

Figure 8. a) Aberration-corrected and monochromated high-resolution TEM image of a C_3N_4@NG hybrid. b) High-resolution TEM image of the same area as in (a) after removal of the g-C_3N_4 layer by electron-beam irradiation. c) The calculated free-energy diagram of the HER at the equilibrium potential for three metal-free catalysts and a Pt reference. d) Polarization curves recorded for the C_3N_4@NG hybrid before and after 1000 potential sweeps under acidic and basic conditions. e) Reaction pathways of the HER on C_3N_4@NG according to the Volmer–Heyrovsky route (upper) and Volmer–Tafel route (bottom). Dashed lines show the activation barriers for each reaction step (reprinted from Ref. [3b] with permission. Copyright 2014 Nature Publishing Group)

those of the g-C_3N_4/NG mixture, which indicates there is a synergistic interaction between g-C_3N_4 and N-doped graphene. DFT calculations were used to establish the selectivity of the potential-dependent pathway on g-C_3N_4@NG: at low overpotentials, the Volmer–Heyrovsky mechanism with electrochemical desorption being the rate-limiting step is the most favorable, whereas the Volmer–Tafel mechanism becomes more favorable at high overpotentials (Figure 8e). By assuming that each reaction step on g-C_3N_4@NG has the same energy barriers as those on a Pt surface, it was found that the Volmer–Tafel mechanism is much faster than the Volmer–Heyrovsky mechanism at low overpotentials, and become equally fast around −1.0 V.

As is the case for other well-studied electrocatalysts (e.g. MoS_2), the defects and edges of g-C_3N_4 are important catalytic centers for water dissociation for the HER. Thus, the assembly of N-doped graphene with porous C_3N_4 (PCN) nanolayers into a 3D free-standing film could lead to a new class of efficient electrocatalysts for the HER. Duan et al. fabricated such a free-standing 3D hybrid film by integrating PCN nanolayers with N-doped graphene sheets (PCN@N-graphene film) by a simple vacuum filtration method (Figure 9a–d).[94] Compared to its 2D counterpart, this 3D heterostructure (Figure 9e) has many intriguing properties for improved catalysis, including highly exposed catalytic centers, hierarchical pores, and strong mechanical flexibility. Electrochemical measurements (Figure 9f) show superior catalytic activities for the HER, with a low overpotential (outperforming previously reported nonmetal electrocatalysts, >200 mV), high exchange current density of 0.43 mA cm^{-2}, and remarkable durability. In a similar but independent study, Qu and co-workers developed an assembled 3D architecture of 1D g-C_3N_4 nanoribbons with 2D graphene sheets (G) by a simple one-step hydrothermal method (Figure 9g,h).[95] This material possesses a large accessible surface area, multielectron transport channel, and short diffusion distance for excellent charge separation and transfer. These unique structural and electronic features led to a high electrocatalytic ability for the HER, with a low onset overpotential of 80 mV, 10 mA cm^{-2} at 207 mV, and a Tafel slope of 54 mV dec^{-1}. Furthermore, Shinde et al. coupled g-C_3N_4 with S and Se codoped porous graphene (pGr) through a scalable approach (Figure 9i).[96] The g-C_3N_4 provided highly active hydrogen adsorption sites, while the S and Se codoped porous graphene facilitated the electron-transfer process for proton reduction (Figure 9j). The high HER performance of the g-C_3N_4@S/SepGr catalyst and a robust stability over a wide pH range indicate the effectiveness of the chemical and electronic coupling to promote proton adsorption and the reduction kinetics. The same authors further synthesized metal-free hybrids by integrating g-C_3N_4 with N and P codoped nanoporous graphene sheets.[97] Other 3D carbon architectures include the HER/OER catalysts based on 2,5-dibromo-3,4-dinitrothiophene (PDNT)/SWCNT com-

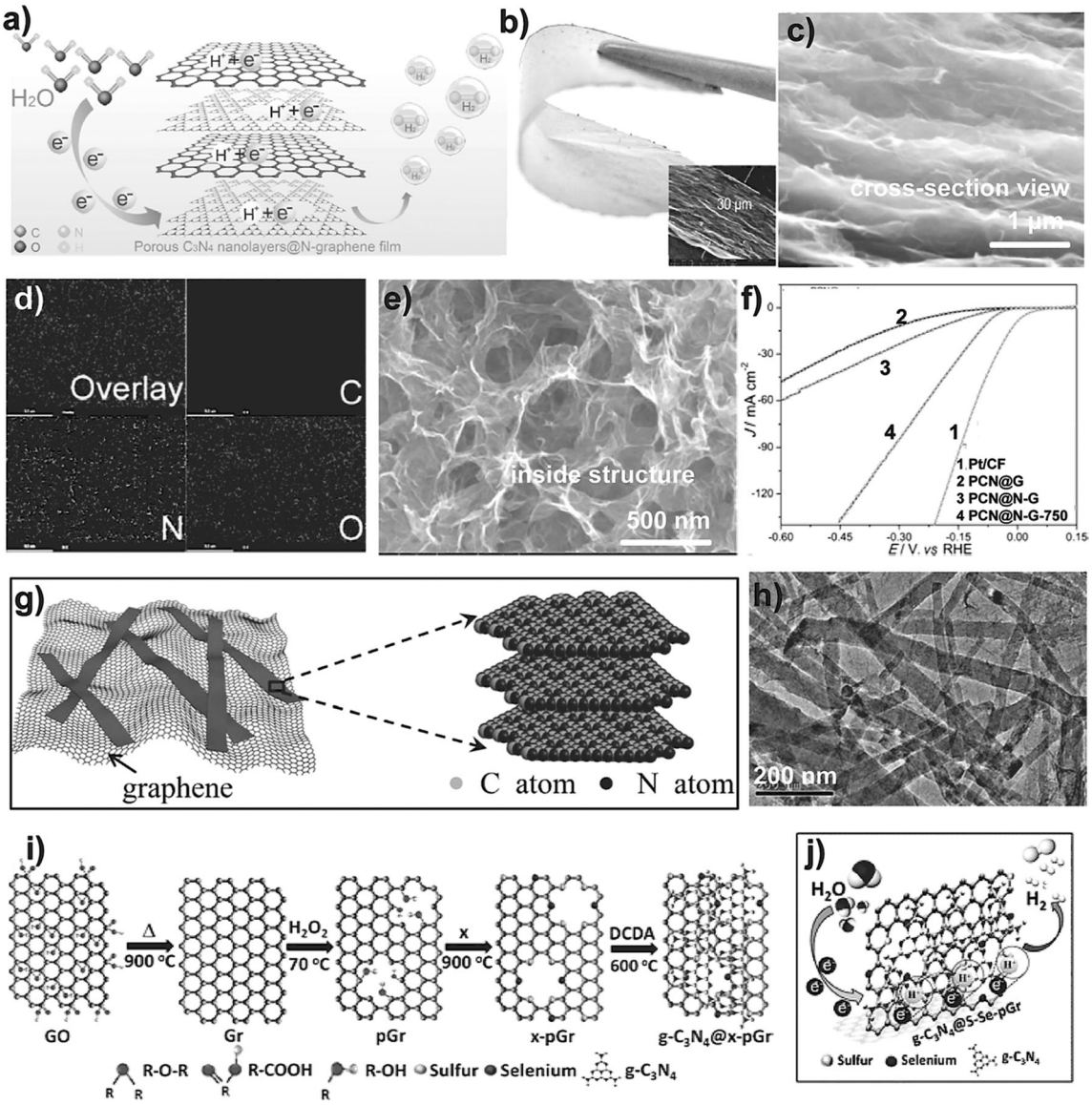

Figure 9. a) Schematic illustration of the HER process of a PCN@N-graphene film. b) Photograph of the PCN@N-graphene film. The inset shows the SEM image of the cross-section. c) SEM image of cross-sectional view. d) EDS overlaid elemental mapping images of C, N, and O as well as individual elements in (c). e) Inner structure of the PCN@N-graphene film. f) Polarization curves of the PCN@graphene, PCN@N-graphene, and PCN@N-graphene-750 films as well as Pt/CF. The inset shows the polarization curves with a current density below 10 mA cm^{-2} (reprinted from Ref. [94] with permission. Copyright 2015 American Chemical Society). g) g-C_3N_4 nanoribbon/G and a possible structural model of the g-C_3N_4 nanoribbon. h) TEM image of the g-C_3N_4 nanoribbon/G (reprinted from Ref. [95] with permission. Copyright 2015 Wiley-VCH). i) Schematic representation of the growth of the hybrid graphene g-C_3N_4@x-pGr (x = S, Se, S-Se). j) Schematic representation of the HER on the g-C_3N_4@S-Se-pGr (reprinted from Ref. [96] with permission. Copyright 2015 Wiley-VCH).

posites,[98] 3D g-C_3N_4/CNT,[99] g-C_3N_4/graphene composites,[100] and P-doped gC_3N_4 (PCN) on a free-standing CF paper.[101] Having both large amounts of functional groups (-OH and -OCO-) and a 3D continuous porous framework, CFP papers are the substrates of choice for the construction of 3D electrodes. Ultrathin g-C_3N_4 nanosheets can provide largely exposed active centers for electrocatalysis, whereas the graphene assembly has a high electrical conductivity for fast charge transport. This, coupled with the porous nature of the CF papers, made the resultant electrode exhibit a greatly enhanced catalytic activity, faster electrocatalytic kinetics, and much better durability for the OER, compared to the IrO_2 electrocatalysts.

More generally, nanoporous 3D carbon architectures with large surface areas could overcome the limitations associated with 1D nanotubes and 2D graphene sheets, and should allow for tunable mechanical and electrical properties that are useful in many potential applications, including electrocatalysis.[6,102] Indeed, Wen et al. have demonstrated that a 3D N-doped carbon nanoarchitecture of N-graphene/CNT hybrids exhibited an outstanding electrocatalytic activity for the OER.[103]

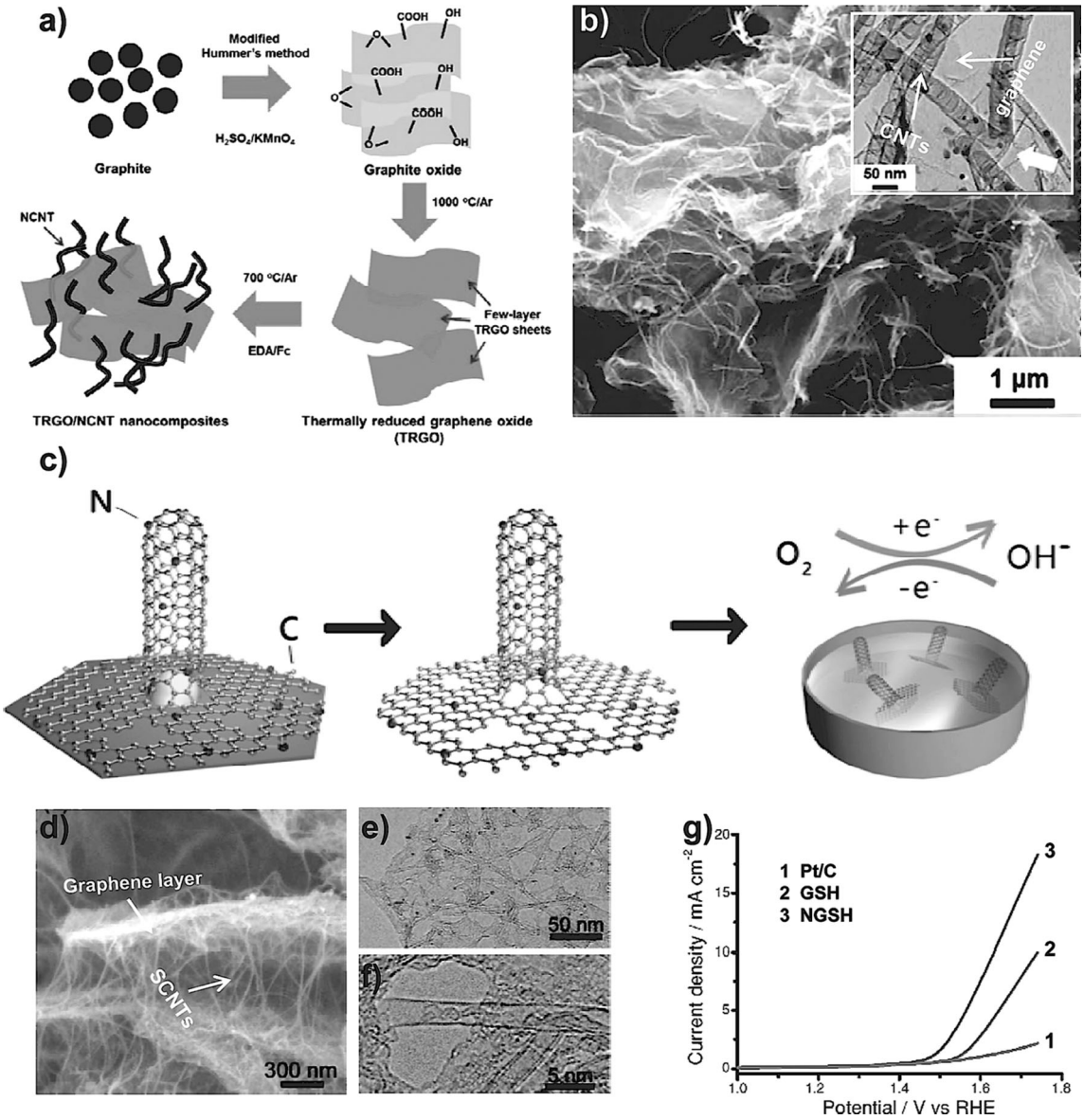

Figure 10. a) Schematic representation of the synthesis of the TRGO/NCNT composite. b) SEM image of TRGO/NCNT; the insert shows the TEM image of TRGO/NCNT (reprinted from Ref. [104] with permission. Copyright 2013ECS, The Electrochemical Society). c) One-step growth of NGSHs for the ORR and OER. d) SEM, e) TEM, and f) high-resolution TEM images of the NGSHs. g) OER currents of Pt/C, GSH, and NGSHs electrodes in 0.1 mol L^{-1} KOH solution at a scan rate of 5 mV s^{-1} (reprinted from Ref. [105] with permission. Copyright 2013 Wiley-VCH).

N-doped CNTs (NCNTs) have also been successfully synthesized on thermally reduced graphene oxide (TRGO) by an injection CVD method. In the formed 3D TRGO/NCNT composite (Figure 10a,b),[104] the NCNTs were utilized to serve as a bridge to electrically connect the discrete graphene sheets for electrical conductivity throughout the electrode and to prevent the graphene sheets from restacking. Furthermore, the NCNTs can also provide catalytically active sites for an efficient OER. By using a layered double hydroxide template, Tian et al. prepared a N-doped graphene/SWCNT hybrid (NGSHs) by in situ doping during CVD growth (Figure 10c).[105] The simultaneous growth of graphene and SWCNTs led to the formation of a 3D interconnected network (Figure 10d–f) with a large specific surface area (812.9 $m^2 g^{-1}$) and high electrical conductivity (53.8 S cm^{-1}). Despite a relatively low N content (0.53 atom %), the 3D NGSHs produced an OER current density of 10 mA cm^{-2} at a potential of 1.63 V (Figure 10g), and a Tafel slope of about 83 mV dec^{-1}, which is much smaller than that of the undoped GSHs and commercial Pt/C. These results demonstrated a high catalytic activity towards the OER for the 3D NGSHs.

4. Carbon-Based Metal-Free OER Catalysts in Metal–Air Batteries

Apart from the important role of carbon-based metal-free catalysts in water-splitting systems, as discussed above, carbon catalysts are also critical to rechargeable metal–air batteries,

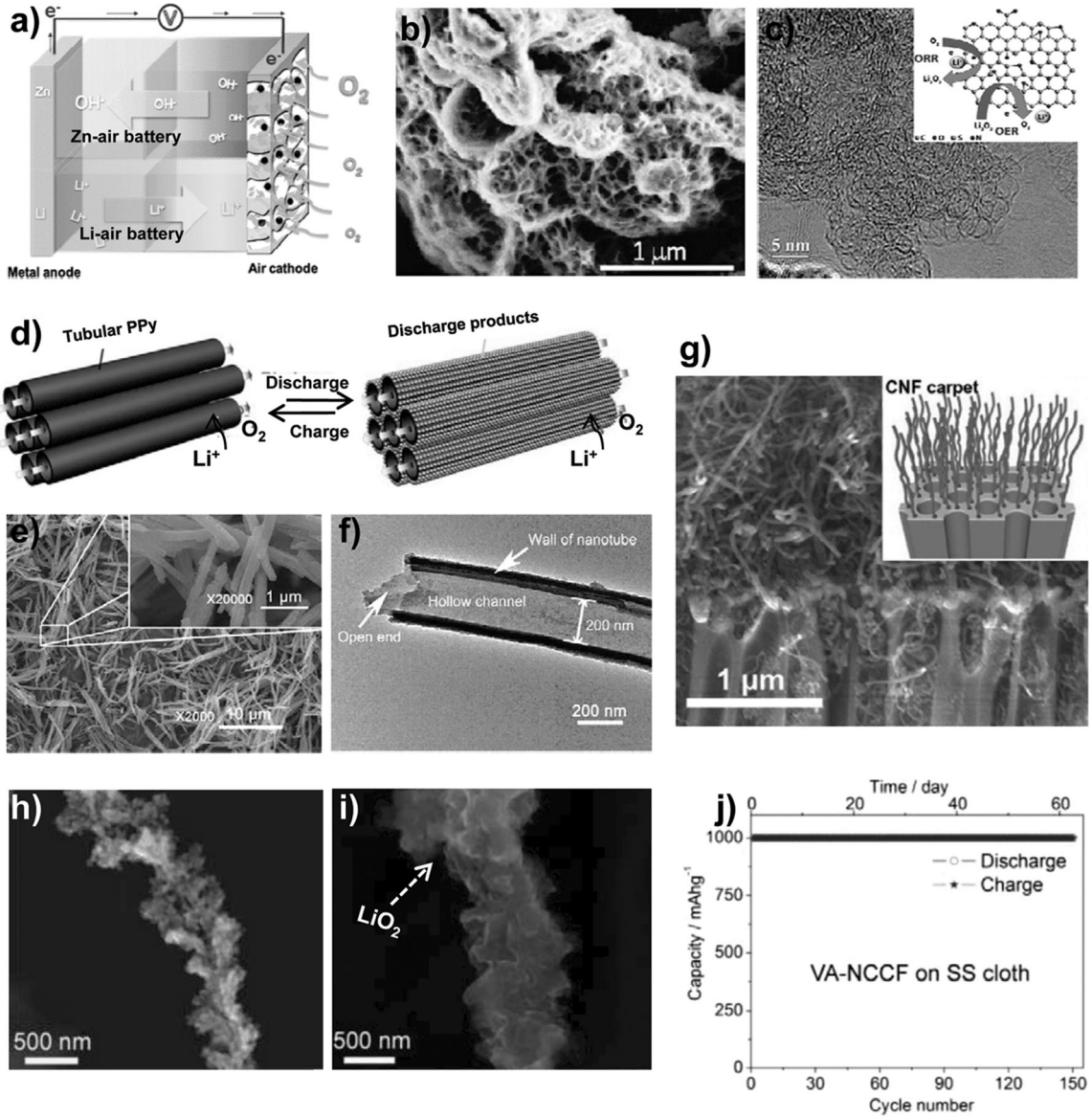

Figure 11. a) Schematic depiction of a metal–air battery (aqueous: Zn–air, non-aqueous: Li–air; reprinted from Ref. [107a] with permission. Copyright 2014 Royal Society of Chemistry). b) SEM images of as-prepared FGS (C/O = 14:1) air electrodes (reprinted from Ref. [111] with permission. Copyright 2011 American Chemical Society). c) High-resolution TEM image of NSGC showing the mesoporous morphology of the rGO surface. The diagram (insert) illustrates the bifunctional catalytic nature of NSGC for the ORR and OER (reprinted from Ref. [113] with permission. Copyright 2015 Royal Society of Chemistry). d) Schematic representations of the discharge/charge process on hydrophilic PPy nanotubes. e) SEM and f) TEM images of the prepared TPPy (reprinted from Ref. [114] with permission. Copyright 2012 Royal Society of Chemistry). g) Cross-sectional (70° tilt) SEM image of the AAO filter after growth of the nanofibers. Inset: schematic representation of the electrode after catalyzed growth of carbon nanofibers (reprinted from Ref. [108a] with permission. Copyright 2011 Royal Society of Chemistry). The formation/decomposition of Li_2O_2 during a discharge/charge cycle on the VA-NCCF fiber: SEM images of h) the pristine fiber, i) the discharged fiber. j) Cycling performance of the VA-NCCF array on the SS cloth substrate (reprinted from Ref. [116] with permission. Copyright 2014 American Chemical Society).

as the OER is at the heart of their function.[106] Typically, metal–air batteries can be divided into two categories according to the nature of the electrolytes: namely, cells with an aqueous electrolyte (e.g. Zn–air) and others with an organic electrolyte (e.g. nonaqueous Li–air; Figure 11 a).[107] In both cases, electrocatalysts for the ORR (discharging) and OER (charging) play a key role in determining the power, energy density, and energy efficiency of the batteries.[107,108] Metal-free carbon-based bifunctional ORR/OER catalysts are, therefore, highly desirable for metal–air batteries. Interestingly, it has been demonstrated that carbon materials can provide sufficient catalytic activity for the ORR in nonaqueous electrolytes.[6,107a] An ideal oxygen electrode in metal–air batteries should have a highly conductive porous structure to facilitate both electron and oxygen transport, plus a large specific surface area for a high Li_2O_2 uptake. In this

context, Yoo and Zhou reported that metal-free graphene nanosheets showed a performance as good as the oxygen electrode in Li–air batteries with a hybrid electrolyte, although their cycling performance needs to be further improved.[109] The high electronic conductivity of the graphene sheets contributed to the low overpotential, while the defects caused by sp^3-bonded carbon atoms in the graphene served as active sites for the ORR and OER.

Sakaushi et al. demonstrated that a mesoporous N-doped carbon based on an ionic liquid can afford efficient metal-free bifunctional catalysis with simultaneous good ORR and OER activities.[110] When used as the cathode in the Li–O_2 system, this material showed a good rate capability with a specific discharge capacity of 1280 mAh g^{-1}, even at a high current density of 200 mA g^{-1}. However, hierarchically porous graphene (Figure 11 b) delivered an exceptionally high capacity of 15000 mAh g^{-1} in Li–O_2 batteries.[111] This is presumably because of the unique bimodal porous structure of the electrode, which consists of microporous channels to facilitate rapid O_2 diffusion and the highly connected nanoscale pores to provide a high density of reactive sites for the Li–O_2 reactions. With the aid of LiI as a redox mediator, Liu et al. have recently demonstrated a high capacity (typically between 25000 to 40000 mAh g^{-1}), comparable to the theoretical value of Li–O_2 batteries, for a RGO framework electrode.[112]

Hybrids of mesoporous carbon on N and S codoped graphene nanosheets (NSGC) with a high active surface area and an enhanced electron/electrolyte conductivity have also been used as an air cathode (Figure 11 c).[113] In this case, the mesoporous structure can accommodate the insoluble Li_2O_2 formed during discharge. As a result, the synthesized NSGC exhibited enhanced bifunctional catalytic activities for the ORR and OER, and also showed a high initial discharge capacity of 11431 mAh g^{-1} and good cycling stability. A highly hydrophilic polypyrrole with a tubular morphology (TPPy), which could build good conductive networks, has also been designed as the air cathode for Li–O_2 batteries.[114] As illustrated in Figure 11 d–f, the high hydrophilicity of the TPPy kept the hollow pores of the nanotubes open and afforded sufficient pathways to transfer O_2 freely to from the inner cathode (Figure 11 d). This leads to uniform distribution of oxygen and deposition of the discharge product. In addition, the proper wettability of the PPy surface allowed the build-up of an organic electrolyte layer with a thickness favorable for the cathodic reaction. Thus, the TPPy air electrode exhibited a higher reversible capacity, higher efficiency, as well as better cycle stability and rate capability than those of a conventional system with acetylene and carbon black.

As the improved contact between the electrode and Li_2O_2 could result in a low overpotential, the continuous coating layer of Li_2O_2 on an electrode is another advantage for the subsequent OER.[115] In this context, Mitchell et al. reported that carbon nanofibers grown on a porous alumina substrate and with a diameter of about 30 nm are promising materials for O_2 electrodes in Li–O_2 batteries.[108a] The aligned carbon nanofibers allowed clear visualization of the Li_2O_2 growth as a function of the depth of discharge as well as disappearance upon charging. These all-carbon-fiber electrodes were found to yield high gravimetric energies (ca. 2500 Wh $kg_{discharged}^{-1}$) in Li–O_2 cells, which is equivalent to a gravimetric energy that is about four times greater than that of the state-of-the-art lithium intercalation electrode (e.g. $LiCoO_2$). The high gravimetric energy density was attributed to low carbon packing in the carbon-fiber electrodes, as well as efficient utilization of the available carbon mass and void volume for Li_2O_2 formation. Recently, Shui et al. prepared vertically aligned nitrogen-doped coral-like carbon nanofiber (VA-NCCF) arrays by CVD and then transferred the as-prepared VA-NCCF onto a piece of microporous stainless-steel (SS) cloth as a binder-free ORR/OER bifunctional electrode for Li–O_2 batteries.[116] The coral-like structure made the continuous coating of Li_2O_2 over the electrode material effective (Figure 11 h,i), and hence led to an extremely narrow voltage gap (0.3 V) between the charge and the discharge plateaus and an unusually high energy efficiency of 90%. As a consequence of the low overpotential of the VA-NCCF electrode, the electrolyte decomposition can be minimized, thereby ensuring a long cycle life of the device. To investigate the stability of the VA-NCCF electrode, the continuous charge/discharge cycling of one cell was performed by using the SS cloth substrate for about 2 months and 150 cycles (Figure 11 j). The cell based on the SS-supported VA-NCCF electrode showed an almost constant capacity of about 1000 mAh g^{-1}. It is the interplay of the N-doping-induced high catalytic activity, the coral-like microstructure, and the highly conductive microporous SS cloth support that endowed the VA-NCCF oxygen electrode with the high performance.

More recently, a 3D N and P codoped mesoporous nanocarbon (NPMC) foam (a bifunctional catalyst for the ORR and OER) was used as the air electrode for primary and rechargeable Zn–air batteries.[81] The primary batteries demonstrated an open-circuit potential of 1.48 V, a specific capacity of 735 mAh g_{Zn}^{-1}, a peak power density of 55 mW cm^{-2}, and stable operation for 240 h after mechanical recharging. Two-electrode rechargeable batteries could be cycled stably over 180 cycles at 2 mA cm^{-2}. These results clearly demonstrated that the performance of metal–air batteries could be dramatically improved by using rationally designed bifunctional ORR/OER electrodes with well-defined hierarchical structures and heteroatom-doping-induced catalytic activities as efficient air cathodes.

5. Conclusions and Outlook

Metal-free carbon-based catalysts hold great promise as efficient HER and OER catalysts to replace precious-metal catalysts for clean energy technologies, including water splitting and metal–air batteries. General strategies for the design of superior catalysts have been summarized, including elemental doping, defect engineering, surface modification, and the fabrication of multidimensional architectures. The materials, charateristics, preparation methods, and the specific performance of the reported metal-free carbon-based catalysts for the HER and OER are compared in Tables 1 and 2.

Table 1: Comparison of materials, charateristics, preparation methods, and specific performance of the carbon-based metal-free HER catalysts.[a]

Samples	Characteristics	Preparation methods	Electrolyte	Onset potential [V]	Potential at 10 mA cm^{-2} [V]	Tafel slope [mV dec^{-1}]	Ref.
N-doped mesoporous graphene	N-doped porous structure	micelle-templating strategy	0.5 M H_2SO_4	−0.15	−0.24	109	[60]
B-substituted graphene	B doping	wet chemical synthetic method	0.5 M H_2SO_4	−0.22	−0.47	99	[69]
activated CNTs	O doping	acidic oxidation and cathodic pre-treatment	0.5 M H_2SO_4	−0.05	−0.22	71.3	[71]
N+S codoped nanoporous graphene	N and S codoping	CVD	0.5 M H_2SO_4	−0.14	−0.39	80.5	[74]
N+S codoped CNTs	N and S codoping	thermal decompositiof peanut root nodules	0.5 M H_2SO_4	−0.05	−0.12	67.8	[75]
N+S codoped porous carbons	N and S codoping	thermal decompositiof hair	0.5 M H_2SO_4	−0.012	−0.097	57.4	[76]
N+P codoped graphene	N and P codoping	pyrolysis of GO with melamine and triphenylphosphine	0.5 M H_2SO_4	−0.2	−0.42	91	[78]
N+P codoped nanoporous graphene	N and P codoping	bottom-up approach (annealing)	0.5 M H_2SO_4	−0.12	−0.213	79	[79]
N+P codoped nanoporous carbon	N and P codoping	$ZnCl_2$ salt and cathodic activation	0.5 M H_2SO_4	−0.076	−0.204	58.4	[80]
N-rich holey graphene monoliths	N doping; holey structure	pyrolysis	0.5 M H_2SO_4 0.1 M KOH	−0.18 −0.30	−0.34 −0.51	99 157	[87]
ordered g-C_3N_4 rods on FTO	structure control	substrate control	0.1 M KOH 0.1 M phosphate buffer	0.0 −0.1	– –	– –	[93]
g-C_3N_4@N-doped graphene	g-C_3N_4/graphene composites; N doping	lyophilization and pyrolysis	0.5 M H_2SO_4 0.1 M KOH	−0.12 −0.35	−0.24 –	51.5 –	[3b]
porous C_3N_4 nanolayers@N-graphene films	g-C_3N_4/graphene composites; porous structure; electrode structure tructure	vacuum filtration method	0.5 M H_2SO_4	−0.008	−0.08	49.1	[94]
g-C_3N_4 nanoribbon-graphene	g-C_3N_4/graphene composites	hydrothermal process	0.5 M H_2SO_4	−0.08	−0.20	54	[95]
g-C_3N_4 and S+Se codoped graphene	g-C_3N_4/graphene composites; S and Se codoping	lyophilization and pyrolysis	0.5 M H_2SO_4 0.1 M KOH	−0.096 −0.45	−0.3 −1.1	86 93	[96]
g-C_3N_4 and N+P codoped graphene	g-C_3N_4/graphene composites; N and P codoping	lyophilization and pyrolysis	0.5 M H_2SO_4 0.1 M KOH	−0.076 −0.45	−0.34 −0.58	90 129	[97]
poly(3,4-dinitrothiophene)/SWCNTs	polymer/CNTs composites	Yamamoto polymerization	1 M H_2SO_4	−0.032	−0.12	–	[98]

[a] –: Data not given. FTO: fluorine-doped tin oxide. All the potentials are calibrated and converted into the reversible hydrogen electrode in this Review.

Table 2: Comparison of the materials, charateristics, preparation methods, and specific performance of the carbon-based metal-free OER catalysts.[a]

Samples	Characteristics	Preparation methods	Electrolyte	onset potential [V]	Potential at 10 mA cm^{-2} [V]	Tafel slope [mV dec^{-1}]	Ref.
CNNTs	N doping	liquid CVD	0.1 M KOH	1.50	1.68	383	[61]
N-doped graphite	N doping	pyrolysis melamine/formaldehyde polymer	0.1 M KOH	1.52	1.61	–	[62]
N-doped graphene (NG)	N doping	pyrolysis of GO and polyaniline	0.1 M KOH	1.41	1.62	–	[63]
N-doped graphene	N doping	hydrothermal method	0.1 M KOH	1.3	–	–	[64]
N-doped carbon sheets	N doping	pyrolysis of chitin	0.1 M KOH	1.06	1.64	116	[65]
B-doped MWCNTs	B doping	CVD	1 M KOH	1.65	1.83	–	[70]
oxidized carbon cloth	O doping	acidic oxidation	0.1 M KOH	1.45	1.72	82	[72]
N+P codoped mesoporous nanocarbon	N and P codoping; porous structure	pyrolysis	0.1 M KOH	1.30	–	–	[81]
N+P codoped graphene/carbon nanosheets	N and P codoping	pyrolysis	0.1 M KOH	1.32	1.57	70	[82]
CNTs with 2–4 walls and 2–5 nm outer diameter	controlled walls and diameter	CVD	1 M KOH	1.64	1.68	60/120	[83]
N-doped coaxial carbon nanocables	controlled "N" distribution	CVD	0.1 M KOH	1.48	1.75	–	[84]
N+O codoped carbon hydrogel film	electrode structure; N and O codoping	layer-by-layer assembly	0.1 M KOH	1.31	1.63	141	[88]
N-doped carbon film	electrode structure; N doping	assembly	0.1 M KOH	1.38	1.42	128	[92]
g-C_3N_4 and CNTs	composites of g-C_3N_4 and CNTs	self-assembly	0.1 M KOH	1.45	1.58	83	[99]
g-C_3N_4/graphene	composites of g-C_3N_4 and graphene	ultrasonication	0.1 M KOH	1.58	1.81	68.5	[100]
P-doped g-C_3N_4 grown on CFP	composites of g-C_3N_4 and carbon; P doping	hydrothermal process	0.1 M KOH	1.53	1.63	61.6	[101]
N-graphene/CNT hybrids	composites of carbon allotropes; N doping	CVD	0.1 M KOH	1.50	1.65	–	[103]
N-doped CNT/graphene composite	composites of carbon allotropes; N doping	injection CVD	0.1 M KOH	1.48	1.65	–	[104]
N-doped graphene/CNTs hybrids	composites of carbon allotropes; N doping	CVD	0.1 M KOH	1.45	1.63	83	[105]
graphene/CNT hybrids	composites of carbon allotropes	CVD	0.1 M KOH	1.52	1.74	97	[105]

[a] GO: graphene oxide. CNNTs: carbon nitrogen nanotubes. CFP: carbon-fiber paper.

Despite significant progress having been made in the area of metal-free carbon-based catalysts for water splitting, the exploration of their applications for other than the ORR is still in its infancy and has multiple challenges. Firstly, the catalytic performance of metal-free carbon-based catalysts still needs to be further improved to meet the requirements for practical applications. Secondly, most studies focus on how to improve the electrocatalytic activity for the HER or OER and ignore the development of a bifunctional electrocatalyst that promotes both high HER and OER activity simultaneously. Most electrocatalysts currently under development for the HER are in acidic electrolytes. The HER performance in alkaline electrolytes is significantly worse because of the inefficient dissociation of water to initiate the Volmer reaction; all OER electrocatalysts available at present only function under alkaline or neutral conditions. This poses a potential problem when the HER is coupled with the OER in the overall water splitting. Thus, finding OER/HER catalysts that can work efficiently over a wide range of pH values has been among the "Holy Grails" of chemistry for a decade, and developing HER catalysts in alkaline media with high performance is highly desirable. The controllable integration of HER and OER catalysts into a nanostructured single metal-free catalyst with high electrocatalytic activities for both the HER and OER is difficult, if not impossible. Opportunities come with challenges; we believe that carbon-based catalysts will soon approach practical applications, particularly in view of the on-going worldwide interest in metal-free catalysis.

[1] a) M. Cabán-Acevedo, M. L. Stone, J. R. Schmidt, J. G. Thomas, Q. Ding, H. C. Chang, M. L. Tsai, J. H. He, S. Jin, *Nat. Mater.* **2015**, *321*, 1245 – 1251; b) J. Q. Tian, Q. Liu, N. Y. Cheng, A. M. Asiri, X. P. Sun, *Angew. Chem. Int. Ed.* **2014**, *53*, 9577 – 9581; *Angew. Chem.* **2014**, *126*, 9731 – 9735; c) W. F. Chen, J. T. Muckerman, E. Fujita, *Chem. Commun.* **2013**, *49*, 8896 – 8909; d) J. D. Benck, T. R. Hellstern, J. Kibsgaard, P. Chakthranont, T. F. Jaramillo, *ACS Catal.* **2014**, *4*, 3957 – 3971.

[2] K. P. Gong, F. Du, Z. H. Xia, M. Durstock, L. M. Dai, *Science* **2009**, *323*, 760 – 764.

[3] a) J. Liu, Y. Liu, N. Y. Liu, Y. Z. Han, X. Zhang, H. Huang, Y. Lifshitz, S. T. Lee, J. Zhong, Z. H. Kang, *Science* **2015**, *347*, 970 – 974; b) Y. Zheng, Y. Jiao, Y. H. Zhu, L. H. Li, Y. Han, Y. Chen, A. J. Du, M. Jaroniec, S. Z. Qiao, *Nat. Commun.* **2014**, *5*, 3783; c) S. Zhang, P. Kang, S. Ubnoske, M. K. Brennaman, N. Song, R. L. House, J. T. Glass, T. J. Meyer, *J. Am. Chem. Soc.* **2014**, *136*, 7845 – 7848; d) B. Kumar, M. Asadi, D. Pisasale, S. Sinha-Ray, B. A. Rosen, R. Haasch, J. Abiade, A. L. Yarin, A. Salehi-khojin, *Nat. Commun.* **2013**, *4*, 2819; e) Y. H. Xue, J. Liu, H. Chen, R. G. Wang, D. Q. Li, J. Qu, L. M. Dai, *Angew. Chem. Int. Ed.* **2012**, *51*, 12124 – 12127; *Angew. Chem.* **2012**, *124*, 12290 – 12293.

[4] a) B. C. H. Steele, A. Heinzel, *Nature* **2001**, *414*, 345 – 352; b) B. Winther-Jensen, O. Winther-Jensen, M. Forsyth, D. R. MacFarlane, *Science* **2008**, *321*, 671 – 674; c) G. Khelashvili, S. Behrens, C. Weidenthaler, C. Vetter, A. Hinsch, R. Kern, K. Skupien, E. Dinjus, H. Bonnemann, *Thin Solid Films* **2006**, *511*, 342 – 348; d) A. Goux, T. Pauporte, D. Lincot, *Electrochim. Acta* **2006**, *51*, 3168 – 3172.

[5] a) Y. Zheng, Y. Jiao, L. Ge, M. Jaroniec, S. Z. Qiao, *Angew. Chem. Int. Ed.* **2013**, *52*, 3110 – 3116; *Angew. Chem.* **2013**, *125*, 3192 – 3198; b) J. Liang, Y. Jiao, M. Jaroniec, S. Z. Qiao, *Angew. Chem. Int. Ed.* **2012**, *51*, 11496 – 11500; *Angew. Chem.* **2012**, *124*, 11664 – 11668; c) R. L. Liu, D. Q. Wu, X. L. Feng, K. Mullen, *Angew. Chem. Int. Ed.* **2010**, *49*, 2565 – 2569; *Angew. Chem.* **2010**, *122*, 2619 – 2623.

[6] L. M. Dai, Y. H. Xue, L. T. Qu, H. J. Choi, J. B. Baek, *Chem. Rev.* **2015**, *115*, 4823 – 4892.

[7] a) H. N. Nong, H. S. Oh, T. Reier, E. Willinger, M. G. Willinger, V. Petkov, D. Teschner, P. Strasser, *Angew. Chem. Int. Ed.* **2015**, *54*, 2975 – 2979; *Angew. Chem.* **2015**, *127*, 3018 – 3022; b) R. Forgie, G. Bugosh, K. C. Neyerlin, Z. C. Liu, P. Strasser, *Electrochem. Solid-State Lett.* **2010**, *13*, B36 – B39; c) T. Reier, M. Oezaslan, P. Strasser, *ACS Catal.* **2012**, *2*, 1765 – 1772; d) A. Bergmann, I. Zaharieva, H. Dau, P. Strasser, *Energy Environ. Sci.* **2013**, *6*, 2745 – 2755.

[8] a) J. K. Nørskov, T. Bligaard, A. Longadottir, J. R. Litchin, J. G. Chen, S. Pandelov, U. Stimming, *J. Electrochem. Soc.* **2005**, *152*, J23 – J26; b) Y. Zheng, Y. Jiao, M. Jaroniec, S. Z. Qiao, *Angew. Chem. Int. Ed.* **2015**, *54*, 52 – 65; *Angew. Chem.* **2015**, *127*, 52 – 66.

[9] a) J. K. Nørskov, T. Bligaard, A. Logadottir, S. Bahn, H. B. Hansen, M. Bollinger, H. Bengaard, B. Hammer, Z. Slijivancanin, M. Mavrikakis, Y. Xu, S. Dahl, C. J. H. Jacobsen, *J. Catal.* **2002**, *209*, 275 – 278; b) Y. Jiao, Y. Zheng, M. Jaroniec, S. Z. Qiao, *Chem. Soc. Rev.* **2015**, *44*, 2060 – 2086.

[10] M. Carmo, D. L. Fritz, J. Mergel, D. Stolten, *Int. J. Hydrogen Energy* **2013**, *38*, 4901 – 4934.

[11] a) J. Rossmeisl, A. Logadottir, J. K. Nørskov, *Chem. Phys.* **2005**, *319*, 178 – 184; b) L. L. Chen, A. Lasia, *J. Electrochem. Soc.* **1991**, *138*, 3460 – 3465.

[12] J. Wu, L. W. Zhu, D. Deng, L. F. Zhu, L. Gu, X. B. Cao, *J. Mater. Chem. A* **2015**, *3*, 11040 – 11047.

[13] N. Zhang, W. G. Ma, T. S. Wu, H. Y. Wang, D. X. Han, L. Niu, *Electrochim. Acta* **2015**, *180*, 155 – 163.

[14] D. S. Kong, J. J. Cha, H. T. Wang, H. R. Lee, Y. Cui, *Energy Environ. Sci.* **2013**, *6*, 3553 – 3558.

[15] X. Long, G. X. Li, Z. L. Wang, H. Y. Zhu, T. Zhang, S. Xiao, W. Y. Guo, S. H. Yang, *J. Am. Chem. Soc.* **2015**, *137*, 11900 – 11903.

[16] H. L. Fei, Y. Yang, X. J. Fan, G. Wang, G. D. Ruan, J. M. Tour, *J. Mater. Chem. A* **2015**, *3*, 5798 – 5804.

[17] L. Yang, X. L. Wu, X. S. Zhu, C. Y. He, M. Meng, Z. X. Gan, P. K. Chu, *Appl. Surf. Sci.* **2015**, *341*, 149 – 156.

[18] Q. F. Gong, L. Cheng, C. H. Liu, M. Zhang, Q. L. Feng, H. L. Ye, M. Zeng, L. M. Xie, Z. Liu, Y. G. Li, *ACS Catal.* **2015**, *5*, 2213 – 2219.

[19] X. B. Chen, Y. Gu, G. H. Tao, Y. L. Pei, G. J. Wang, N. Cui, *J. Mater. Chem. A* **2015**, *3*, 18898 – 18905.

[20] X. W. Zhang, F. Meng, S. Mao, Q. Ding, M. J. Shearer, M. S. Faber, J. H. Chen, R. J. Hamers, S. Jin, *Energy Environ. Sci.* **2015**, *8*, 862 – 868.

[21] P. Jiang, Q. Liu, Y. Liang, J. Tian, A. M. Asiri, X. Sun, *Angew. Chem. Int. Ed.* **2014**, *53*, 12855 – 12859; *Angew. Chem.* **2014**, *126*, 13069 – 13073.

[22] a) E. J. Popczun, J. R. McKone, C. G. Read, A. J. Biacchi, A. M. Wiltrout, N. S. Lewis, R. E. Schaak, *J. Am. Chem. Soc.* **2013**, *135*, 9267 – 9270; b) Z. Huang, Z. Chen, Z. Chen, C. Lv, H. Meng, C. Zhang, *ACS Nano* **2014**, *8*, 8121 – 8129; c) A. B. Laursen, K. R. Patraju, M. J. Whitaker, M. Retuerto, T. Sarkar, N. Yao, K. V. Ramanujachary, M. Greenblatt, G. C. Dismukes, *Energy Environ. Sci.* **2015**, *8*, 1027 – 1034.

[23] a) A. Lu, Y. Chen, H. Li, A. Dowd, M. B. Cortie, Q. Xie, H. Guo, Q. Qi, D. L. Peng, *Int. J. Hydrogen Energy* **2014**, *39*, 18919 – 18928; b) E. J. Popczun, C. G. Read, C. W. Roske, N. S. Lewis, R. E. Schaak, *Angew. Chem. Int. Ed.* **2014**, *53*, 5427 –

5430; *Angew. Chem.* **2014**, *126*, 5531 – 5534; c) Q. Liu, J. Tian, W. Cui, P. Jiang, N. Cheng, A. M. Asiri, X. Sun, *Angew. Chem. Int. Ed.* **2014**, *53*, 6710 – 6714; *Angew. Chem.* **2014**, *126*, 6828 – 6832.
[24] P. Xiao, M. A. Sk, L. Thia, X. Ge, R. J. Lim, J. Y. Wang, K. H. Lim, X. Wang, *Energy Environ. Sci.* **2014**, *7*, 2624 – 2629.
[25] F. Rosalbino, S. Delsante, G. Borzone, E. Angelini, *Int. J. Hydrogen Energy* **2008**, *33*, 6696 – 6703.
[26] P. P. Li, Z. Y. Jin, D. Xiao, *J. Mater. Chem. A* **2014**, *2*, 18420 – 18427.
[27] D. Gopalakrishnan, D. Damien, M. M. Shaijumon, *ACS Nano* **2014**, *8*, 5297 – 5303.
[28] S. J. Xu, Z. Y. Lei, P. Y. Wu, *J. Mater. Chem. A* **2015**, *3*, 16337 – 16347.
[29] P. Zhang, T. Tachikawa, M. Fujitsuka, T. Majima, *Chem. Commun.* **2015**, *51*, 7187 – 7190.
[30] M. K. Bates, Q. Y. Jia, N. Ramaswamy, R. J. Allen, S. Mukerjee, *J. Phys. Chem. C* **2015**, *119*, 5467 – 5477.
[31] A. Le Goff, V. Artero, B. Jousselme, P. D. Tran, N. Guillet, R. Métayé, A. Fihri, S. Palacin, M. Fontecave, *Science* **2009**, *326*, 1384 – 1387.
[32] X. Liu, S. S. Cui, Z. J. Sun, P. W. Du, *Chem. Commun.* **2015**, *51*, 12954 – 12957.
[33] J. S. Qin, D. Y. Du, W. Guan, X. J. Bo, Y. F. Li, L. P. Guo, Z. M. Su, Y. Y. Wang, Y. Q. Lan, H. C. Zhou, *J. Am. Chem. Soc.* **2015**, *137*, 7169 – 7177.
[34] a) Y. Liang, Y. Li, H. Wang, J. Zhou, J. Wang, T. Regier, H. Dai, *Nat. Mater.* **2011**, *10*, 780 – 786; b) Y. Sun, S. Gao, F. Lei, J. Liu, L. Liang, Y. Xie, *Chem. Sci.* **2014**, *5*, 3976 – 3982; c) R. D. Smith, M. S. Prévot, R. D. Fagan, Z. Zhang, P. A. Sedach, M. K. J. Siu, S. Trudel, C. P. Berlinguette, *Science* **2013**, *340*, 60 – 63; d) A. Grimaud, K. J. May, C. E. Carlton, Y. L. Lee, M. Risch, W. T. Hong, J. Zhou, Y. Shao-Horn, *Nat. Commun.* **2013**, *4*, 2439; e) Z. Peng, D. Jia, A. Al-Enizi, A. Elzatahry, G. Zheng, *Adv. Energy Mater.* **2015**, *5*, 1402031; f) R. Subbaraman, D. Tripkovic, K. C. Chang, D. Strmcnik, A. P. Paulikas, P. Hirunsit, M. Chan, J. Greeley, V. Stamenkovic, N. M. Markovic, *Nat. Mater.* **2012**, *11*, 550 – 557; g) T. L. Wee, B. D. Sherman, D. Gust, A. L. Moore, T. A. Moore, Y. Liu, J. C. Scaiano, *J. Am. Chem. Soc.* **2011**, *133*, 16742 – 16745; h) J. Rosen, G. S. Hutchings, F. Jiao, *J. Am. Chem. Soc.* **2013**, *135*, 4516 – 4521; i) J. Ryu, N. Jung, J. H. Jang, H. J. Kim, S. J. Yoo, *ACS Catal.* **2015**, *5*, 4066 – 4074; j) Y. R. Zheng, M. R. Gao, Q. Gao, H. H. Li, J. Xu, Z. Y. Wu, S. H. Yu, *Small* **2015**, *11*, 182 – 188.
[35] L. H. Wu, Q. Li, C. H. Wu, H. Y. Zhu, A. Mendoza-Garcia, B. Shen, J. H. Guo, S. H. Sun, *J. Am. Chem. Soc.* **2015**, *137*, 7071 – 7074.
[36] a) V. Artero, M. Chavarot-Kerlidou, M. Fontecave, *Angew. Chem. Int. Ed.* **2011**, *50*, 7238 – 7266; *Angew. Chem.* **2011**, *123*, 7376 – 7405; b) J. A. Koza, Z. He, A. S. Miller, J. A. Switzer, *Chem. Mater.* **2012**, *24*, 3567 – 3573.
[37] a) G. S. Hutchings, Y. Zhang, J. Li, B. T. Yonemoto, X. G. Zhou, K. K. Zhu, F. Jiao, *J. Am. Chem. Soc.* **2015**, *137*, 4223 – 4229; b) M. Hamdani, R. Singh, P. Chartier, *Int. J. Electrochem. Sci.* **2010**, *5*, 556 – 577; c) X. Lu, C. Zhao, *J. Mater. Chem. A* **2013**, *1*, 12053 – 12059.
[38] C. Z. Zhu, D. Wen, S. Leubner, M. Oschatz, W. Liu, M. Holzschuh, F. Simon, S. Kaskel, A. Eychmüller, *Chem. Commun.* **2015**, *51*, 7851 – 7854.
[39] a) Y. Li, P. Hasin, Y. Wu, *Adv. Mater.* **2010**, *22*, 1926 – 1929; b) S. Chen, J. J. Duan, M. Jaroniec, S. Z. Qiao, *Angew. Chem. Int. Ed.* **2013**, *52*, 13567 – 13570; *Angew. Chem.* **2013**, *125*, 13812 – 13815.
[40] J. Wang, T. Qiu, X. Chen, Y. L. Lu, W. S. Yang, *J. Power Sources* **2014**, *268*, 341 – 348.
[41] a) L. Trotochaud, J. K. Ranney, K. N. Williams, S. W. Boettcher, *J. Am. Chem. Soc.* **2012**, *134*, 17253 – 17261; b) C. C. L. McCrory, S. H. Jung, J. C. Peters, T. F. Jaramillo, *J. Am. Chem. Soc.* **2013**, *135*, 16977 – 16987.
[42] M. W. Kanan, D. G. Nocera, *Science* **2008**, *321*, 1072 – 1075.
[43] Y. C. Wang, K. Jiang, H. Zhang, T. Zhou, J. W. Wang, W. Wei, Z. Q. Yang, X. H. Sun, W. B. Cai, G. F. Zheng, *Adv. Sci.* **2015**, *2*, 1500003.
[44] a) I. Nikolov, R. Darkaoui, E. Zhecheva, R. Stoyanova, N. Dimitrov, T. Vitanov, *J. Electroanal. Chem.* **1997**, *429*, 157 – 168.
[45] Z. B. Zhuang, W. C. Sheng, Y. S. Yan, *Adv. Mater.* **2014**, *26*, 3950 – 3955.
[46] M. Gong, W. Zhou, M. C. Tsai, J. Zhou, M. Guan, M. C. Lin, B. Zhang, Y. Hu, D. Y. Wang, J. Yang, S. J. Pennycook, B. J. Hwang, H. J. Dai, *Nat. Commun.* **2014**, *5*, 4695.
[47] J. Suntivich, K. J. May, H. A. Gasteiger, J. B. Goodenough, Y. Shao-Horn, *Science* **2011**, *334*, 1383 – 1385.
[48] R. D. L. Smith, M. S. Prévot, R. D. Fagan, S. Trudel, C. P. Berlinguette, *J. Am. Chem. Soc.* **2013**, *135*, 11580 – 11586.
[49] W. Zhou, X. J. Wu, X. Cao, X. Huang, C. Tan, J. Tian, H. Liu, J. Wang, H. Zhang, *Energy Environ. Sci.* **2013**, *6*, 2921 – 2924.
[50] M. Ledendecker, S. Krick Calderón, C. Papp, H. P. Steinrück, M. Antonietti, M. Shalom, *Angew. Chem. Int. Ed.* **2015**, *54*, 12361 – 12365; *Angew. Chem.* **2015**, *127*, 12538 – 12542.
[51] M. R. Gao, X. Cao, Q. Gao, Y. F. Xu, Y. R. Zheng, J. Jiang, S. H. Yu, *ACS Nano* **2014**, *8*, 3970 – 3978.
[52] D. Merki, S. Fierro, H. Vrubel, X. Hu, *Chem. Sci.* **2011**, *2*, 1262 – 1267.
[53] a) Q. Li, P. Xu, B. Zhang, H. Tsai, J. Wang, H. L. Wang, G. Wu, *Chem. Commun.* **2013**, *49*, 10838 – 10840; b) Q. G. He, Q. Li, S. Khene, X. M. Ren, F. E. Lopez-Suarez, D. Lozano-Castello, A. Bueno-Lopez, G. Wu, *J. Phys. Chem. C* **2013**, *117*, 8697 – 8707; c) Q. Li, P. Xu, W. Gao, S. Ma, G. Zhang, R. Cao, J. Cho, H. L. Wang, G. Wu, *Adv. Mater.* **2014**, *26*, 1378 – 1386.
[54] a) S. Chen, J. J. Duan, J. R. Ran, M. Jaroniec, S. Z. Qiao, *Energy Environ. Sci.* **2013**, *6*, 3693 – 3699; b) M. Gong, Y. G. Li, H. L. Wang, Y. Y. Liang, J. Z. Wu, J. G. Zhou, J. Wang, T. Regier, F. Wei, H. J. Dai, *J. Am. Chem. Soc.* **2013**, *135*, 8452 – 8455; c) X. Long, J. K. Li, S. Xiao, K. Y. Yan, Z. L. Wang, H. N. Chen, S. H. Yang, *Angew. Chem. Int. Ed.* **2014**, *53*, 7584 – 7588; *Angew. Chem.* **2014**, *126*, 7714 – 7718; d) X. E. Liu, W. Liu, M. Ko, M. Park, M. G. Kim, P. Oh, S. Chae, S. Park, A. Casimir, G. Wu, J. Cho, *Adv. Funct. Mater.* **2015**, *25*, 5799 – 5808; e) X. J. Fan, Z. W. Peng, R. Q. Ye, H. Q. Zhou, X. Guo, *ACS Nano* **2015**, *9*, 7407 – 7418; f) M. Tavakkoli, T. Kallio, O. Reynaud, A. G. Nasibulin, C. Johans, J. Sainio, H. Jiang, E. I. Kauppinen, K. Laasonen, *Angew. Chem. Int. Ed.* **2015**, *54*, 4535 – 4538; *Angew. Chem.* **2015**, *127*, 4618 – 4621; g) T. N. Ye, L. B. Lv, M. Xu, B. Zhang, K. X. Wang, J. Su, X. H. Lin, J. S. Chen, *Nano Energy* **2015**, *15*, 335 – 342.
[55] C. G. Hu, Y. Xiao, Y. Zhao, N. Chen, Z. P. Zhang, M. H. Cao, L. T. Qu, *Nanoscale* **2013**, *5*, 2726 – 2733.
[56] a) Q. Wen, W. Z. Qian, J. Q. Nie, A. Y. Cao, G. Q. Ning, Y. Wang, L. Hu, Q. Zhang, J. Q. Huang, F. Wei, *Adv. Mater.* **2010**, *22*, 1867 – 1871; b) R. F. Zhang, Y. Y. Zhang, Q. Zhang, H. H. Xie, W. Z. Qian, F. Wei, *ACS Nano* **2013**, *7*, 6156 – 6161; c) C. Li, G. Q. Shi, *Adv. Mater.* **2014**, *26*, 3992 – 4012; d) C. Lee, X. D. Wei, J. W. Kysar, J. Hone, *Science* **2008**, *321*, 385 – 388; e) R. R. Nair, P. Blake, A. N. Grigorenko, K. S. Novoselov, T. J. Booth, T. Stauber, N. M. R. Peres, A. K. Geim, *Science* **2008**, *320*, 1308 – 1308; f) L. T. Qu, Y. Liu, J. B. Baek, L. M. Dai, *ACS Nano* **2010**, *4*, 1321 – 1326; g) C. G. Hu, L. Song, Z. P. Zhang, N. Chen, Z. H. Feng, L. T. Qu, *Energy Environ. Sci.* **2015**, *8*, 31 – 54; h) X. Wang, L. J. Zhi, N. Tsao, Z. Tomovic, J. L. Li, K. Mullen, *Angew. Chem. Int. Ed.* **2008**, *47*, 2990 – 2992; *Angew. Chem.* **2008**, *120*, 3032 – 3034; i) C. G. Hu, H. H. Cheng, Y. Zhao, Y. Hu, Y. Liu, L. M. Dai, L. T. Qu, *Adv. Mater.* **2012**, *24*, 5493 – 5498.

[57] a) L. M. Dai, *Acc. Chem. Res.* **2013**, *46*, 31 – 42; b) J. T. Zhang, L. M. Dai, *ACS Catal.* **2015**, *5*, 7244 – 7253; c) X. Sun, P. Song, Y. Zhang, C. Liu, W. Xu, W. Xing, *Sci. Rep.* **2013**, *3*, 2505; d) Z. Liu, F. Peng, H. Wang, H. Yu, J. Tan, L. Zhu, *Catal. Commun.* **2011**, *16*, 35 – 38; e) D. Geng, Y. Chen, Y. Chen, Y. Li, R. Li, X. Sun, S. Ye, S. Knights, *Energy Environ. Sci.* **2011**, *4*, 760 – 764.

[58] a) R. S. Lee, H. J. Kim, J. E. Fischer, A. Thess, R. E. Smalley, *Nature* **1997**, *388*, 255 – 257; b) P. Avouris, Z. H. Chen, V. Perebeinos, *Nat. Nanotechnol.* **2007**, *2*, 605 – 615; c) J. J. Duan, S. Chen, M. Jaroniec, S. Z. Qiao, *ACS Catal.* **2015**, *5*, 5207 – 5234.

[59] a) K. N. Wood, R. O'Hayre, S. Pylypenko, *Energy Environ. Sci.* **2014**, *7*, 1212 – 1249; b) X. Lepró, R. Ovalle-Robles, M. D. Lima, A. L. Elias, M. Terrones, R. H. Baughman, *Adv. Funct. Mater.* **2012**, *22*, 1069 – 1075.

[60] X. D. Huang, Y. F. Zhao, Z. M. Ao, G. X. Wang, *Sci. Rep.* **2014**, *4*, 7557.

[61] R. M. Yadav, J. J. Wu, R. Kochandra, L. Ma, C. S. Tiwary, L. H. Ge, G. L. Ye, R. Vajtai, J. Lou, P. M. Ajayan, *ACS Appl. Mater. Interfaces* **2015**, *7*, 11991 – 12000.

[62] Y. Zhao, R. H. Nakamura, K. Kamiya, S. J. Nakanishi, K. Hashimoto, *Nat. Commun.* **2013**, *4*, 2390.

[63] Z. Y. Lin, G. H. Waller, Y. Liu, M. L. Liu, C. P. Wong, *Carbon* **2013**, *53*, 130 – 136.

[64] L. Wang, F. X. Yin, C. X. Yao, *Int. J. Hydrogen Energy* **2014**, *39*, 15913 – 15919.

[65] H. R. Yuan, L. F. Deng, X. X. Cai, S. G. Zhou, Y. Chen, Y. Yuan, *RSC Adv.* **2015**, *5*, 56121 – 56129.

[66] a) P. Redlich, J. Loeffler, P. M. Ajayan, J. Bill, F. Aldinger, M. Ruhle, *Chem. Phys. Lett.* **1996**, *260*, 465 – 470; b) W. Q. Han, Y. Bando, K. Kurashima, T. Sato, *Chem. Phys. Lett.* **1999**, *299*, 368 – 373.

[67] B. Q. Wei, R. Spolenak, P. Kohler-Redlich, M. Ruhle, E. Arzt, *Appl. Phys. Lett.* **1999**, *74*, 3149 – 3151.

[68] K. C. Mondal, A. M. Strydom, R. M. Erasmus, J. M. Keartland, N. J. Coville, *Mater. Chem. Phys.* **2008**, *111*, 386 – 390.

[69] B. R. Sathe, X. X. Zou, T. Asefa, *Catal. Sci. Technol.* **2014**, *4*, 2023 – 2030.

[70] Y. H. Cheng, Y. Y. Tian, X. Z. Fan, J. G. Liu, C. W. Yan, *Electrochim. Acta* **2014**, *143*, 291 – 296.

[71] N. Y. Cheng, Q. Liu, J. Q. Tian, Y. R. Xue, A. M. Asiri, H. F. Jiang, Y. Q. Hee, X. P. Sun, *Chem. Commun.* **2014**, *50*, 9340 – 9342.

[72] N. Y. Cheng, Q. Liu, J. Q. Tian, Y. R. Xue, A. M. Asiri, H. F. Jiang, Y. Q. Hee, X. P. Sun, *Chem. Commun.* **2015**, *51*, 1616 – 1619.

[73] a) X. Gong, S. Liu, C. Ouyang, P. Strasser, R. Yang, *ACS Catal.* **2015**, *5*, 920 – 927; b) C. H. Choi, M. W. Chung, S. H. Park, S. I. Woo, *Phys. Chem. Chem. Phys.* **2013**, *15*, 1802 – 1805; c) C. H. Choi, M. W. Chuang, H. C. Kwon, S. H. Park, S. I. Woo, *J. Mater. Chem. A* **2013**, *1*, 3694 – 3699.

[74] Y. Ito, W. T. Cong, T. Fujita, Z. Tang, M. W. Chen, *Angew. Chem. Int. Ed.* **2015**, *54*, 2131 – 2136; *Angew. Chem.* **2015**, *127*, 2159 – 2164.

[75] Y. C. Zhou, Y. H. Leng, W. J. Zhou, J. L. Huang, M. W. Zhao, J. Zhan, C. H. Feng, Z. H. Tang, S. W. Chen, H. Liu, *Nano Energy* **2015**, *16*, 357 – 366.

[76] X. J. Liu, W. J. Zhou, L. J. Yang, L. G. Li, Z. Y. Zhang, Y. T. Ke, S. W. Che, *J. Mater. Chem. A* **2015**, *3*, 8840 – 8846.

[77] a) Z. W. Liu, F. Peng, H. J. Wang, H. Yu, W. X. Zheng, J. A. Yang, *Angew. Chem. Int. Ed.* **2011**, *50*, 3257 – 3261; *Angew. Chem.* **2011**, *123*, 3315 – 3319; b) Y. Zheng, Y. Jiao, S. Z. Qiao, *Adv. Mater.* **2015**, *27*, 5372 – 5378.

[78] Y. Zheng, Y. Jiao, L. H. Li, T. Xing, Y. Chen, M. Jaroniec, S. Z. Qiao, *ACS Nano* **2014**, *8*, 5290 – 5296.

[79] H. L. Jiang, Y. H. Zhu, Y. H. Su, Y. F. Yao, Y. Y. Liu, X. L. Yang, C. Z. Li, *J. Mater. Chem. A* **2015**, *3*, 12642 – 12645.

[80] L. Wei, H. E. Karahan, K. Goh, W. C. Jiang, D. S. Yu, Ö. Birer, R. R. Jiang, Y. Chen, *J. Mater. Chem. A* **2015**, *3*, 7210 – 7214.

[81] J. T. Zhang, Z. H. Zhao, Z. H. Xia, L. M. Dai, *Nat. Nanotechnol.* **2015**, *10*, 444 – 452.

[82] R. Li, Z. D. Wei, X. L. Gou, *ACS Catal.* **2015**, *5*, 4133 – 4142.

[83] Y. Cheng, C. W. Xu, L. C. Jia, J. L. D. Gale, L. L. Zhang, C. Liu, P. K. Shen, S. P. Jiang, *Appl. Catal. B* **2015**, *163*, 96 – 104.

[84] G. L. Tian, Q. Zhang, B. S. Zhang, Y. G. Jin, J. Q. Huang, D. S. Su, F. Wei, *Adv. Funct. Mater.* **2014**, *24*, 5956 – 5961.

[85] a) G. C. Xie, K. Zhang, B. D. Guo, Q. Liu, L. Fang, J. R. Gong, *Adv. Mater.* **2013**, *25*, 3820 – 3839; b) I. Katsounaros, S. Cherevko, A. R. Zeradjanin, K. J. J. Mayrhofer, *Angew. Chem. Int. Ed.* **2014**, *53*, 102 – 121; *Angew. Chem.* **2014**, *126*, 104 – 124.

[86] P. F. Zhang, Z. A. Qiao, Z. Y. Zhang, S. Wan, S. Dai, *J. Mater. Chem. A* **2014**, *2*, 12262 – 12269.

[87] J. M. Ge, B. Zhang, L. B. Lv, H. H. Wang, T. N. Ye, X. Wei, J. Su, K. X. Wang, X. H. Lin, J. S. Chen, *Nano Energy* **2015**, *15*, 567 – 575.

[88] S. Chen, J. J. Duan, M. Jaroniec, S. Z. Qiao, *Adv. Mater.* **2014**, *26*, 2925 – 2930.

[89] Y. Luo, J. Jiang, W. Zhou, H. Yang, J. Luo, X. Qi, H. Zhang, D. Y. W. Yu, C. M. Li, T. Yu, *J. Mater. Chem.* **2012**, *22*, 8634 – 8640.

[90] J. D. Roy-Mayhew, G. Boschloo, A. Hagfeldt, I. A. Aksay, *ACS Appl. Mater. Interfaces* **2012**, *4*, 2794 – 2800.

[91] Z. Zhao, H. Wu, H. He, X. Xu, Y. Jin, *Adv. Funct. Mater.* **2014**, *24*, 4698 – 4705.

[92] S. Chen, J. J. Duan, J. R. Ran, S. Z. Qiao, *Adv. Sci.* **2015**, *2*, 1400015.

[93] M. Shalom, S. Gimenez, F. Schipper, I. Herraiz-Cardona, J. Bisquert, M. Antonietti, *Angew. Chem. Int. Ed.* **2014**, *53*, 3654 – 3658; *Angew. Chem.* **2014**, *126*, 3728 – 3732.

[94] J. J. Duan, S. Chen, M. Jaroniec, S. Z. Qiao, *ACS Nano* **2015**, *9*, 931 – 940.

[95] Y. Zhao, F. Zhao, X. P. Wang, C. Y. Xu, Z. P. Zhang, G. Q. Shi, L. T. Qu, *Angew. Chem. Int. Ed.* **2014**, *53*, 13934 – 13939; *Angew. Chem.* **2014**, *126*, 14154 – 14159.

[96] S. S. Shinde, A. Sami, J. H. Lee, *J. Mater. Chem. A* **2015**, *3*, 12810 – 12819.

[97] S. S. Shinde, A. Sami, J. H. Lee, *ChemCatChem* **2015**, *7*, 3873 – 3880.

[98] K. Xie, H. P. Wu, Y. N. Meng, K. Lu, Z. X. Wei, Z. Zhang, *J. Mater. Chem. A* **2015**, *3*, 78 – 82.

[99] T. Y. Ma, S. Dai, M. Jaroniec, S. Z. Qiao, *Angew. Chem. Int. Ed.* **2014**, *53*, 7281 – 7285; *Angew. Chem.* **2014**, *126*, 7409 – 7413.

[100] J. Q. Tian, Q. Liu, A. M. Asiri, K. A. Alamry, X. P. Sun, *ChemSusChem* **2014**, *7*, 2125 – 2132.

[101] T. Y. Ma, J. R. Ran, S. Dai, M. Jaroniec, S. Z. Qiao, *Angew. Chem. Int. Ed.* **2015**, *54*, 4646 – 4650; *Angew. Chem.* **2015**, *127*, 4729 – 4733.

[102] W. Wei, Y. Tao, W. Lv, F. Y. Su, L. Ke, J. Li, D. W. Wang, B. H. Li, F. Y. Kang, Q. H. Yang, *Sci. Rep.* **2014**, *4*, 6289.

[103] Z. H. Wen, S. Q. Ci, Y. Hou, J. H. Chen, *Angew. Chem. Int. Ed.* **2014**, *53*, 6496 – 6500; *Angew. Chem.* **2014**, *126*, 6614 – 6618.

[104] H. W. Park, D. U. Lee, Y. L. Liu, J. Wu, L. F. Nazar, Z. W. Chen, *J. Electrochem. Soc.* **2013**, *160*, A2244 – A2250.

[105] G. L. Tian, M. Q. Zhao, D. S. Yu, X. Y. Kong, J. Q. Huang, Q. Zhang, F. Wei, *Small* **2014**, *10*, 2251 – 2259.

[106] Q. Li, R. G. Cao, J. Cho, G. Wu, *Adv. Energy Mater.* **2014**, *4*, 1301415.

[107] a) Z. L. Wang, D. Xu, J. J. Xu, X. B. Zhang, *Chem. Soc. Rev.* **2014**, *43*, 7746 – 7786; b) S. M. Zhu, Z. Chen, B. Li, D. Higgins, H. J. Wang, H. Li, Z. W. Chen, *Electrochim. Acta* **2011**, *56*, 5080 – 5084.

[108] a) R. R. Mitchell, B. M. Gallant, C. V. Thompson, Y. Shao-Horn, *Energy Environ. Sci.* **2011**, *4*, 2952 – 2958; b) Y. C. Lu, Z. C. Xu, H. A. Gasteiger, S. Chen, K. Hamad-Schifferli, Y.

Shao-Horn, *J. Am. Chem. Soc.* **2010**, *132*, 12170 – 12171; c) Q. Li, R. G. Cao, J. Cho, G. Wu, *Phys. Chem. Chem. Phys.* **2014**, *16*, 13568 – 13582.
[109] E. Yoo, H. S. Zhou, *ACS Nano* **2011**, *5*, 3020 – 3026.
[110] K. Sakaushi, T. P. Fellinger, M. Antonietti, *ChemSusChem* **2015**, *8*, 1156 – 1160.
[111] J. Xiao, D. H. Mei, X. L. Li, W. Xu, D. Y. Wang, G. L. Graff, W. D. Bennett, Z. M. Nie, L. V. Saraf, I. A. Aksay, J. Liu, J. G. Zhang, *Nano Lett.* **2011**, *11*, 5071 – 5078.
[112] T. Liu, M. Leskes, W. J. Yu, A. J. Moore, L. N. Zhou, P. M. Bayley, G. W. Kim, C. P. Grey, *Science* **2015**, *350*, 530 – 533.
[113] J. H. Kim, A. G. Kannan, H. S. Woo, D. G. Jin, W. Kim, K. Ryu, D. W. Kim, *J. Mater. Chem. A* **2015**, *3*, 18456 – 18465.
[114] Y. M. Cui, Z. Y. Wen, X. Liang, Y. Lu, J. Jin, M. F. Wu, X. W. Wu, *Energy Environ. Sci.* **2012**, *5*, 7893 – 7897.
[115] a) E. Yilmaz, C. Yogi, K. Yamanaka, T. Ohta, H. R. Byon, *Nano Lett.* **2013**, *13*, 4679 – 4684; b) H. D. Lim, H. Song, H. Gwon, K. Y. Park, J. Kim, Y. Bae, H. Kim, S. K. Jung, T. Kim, Y. H. Kim, X. Lepro, R. Ovalle-Robles, R. H. Baughman, K. Kang, *Energy Environ. Sci.* **2013**, *6*, 3570 – 3575.
[116] J. L. Shui, F. Du, C. M. Xue, Q. Li, L. M. Dai, *ACS Nano* **2014**, *8*, 3015 – 3022.

Received: October 26, 2015
Published online: ■■ ■■, ■■■■

Reviews

Electrocatalysis

C. Hu, L. Dai* _____ ■■■■–■■■■

Carbon-Based Metal-Free Catalysts for Electrocatalysis beyond the ORR

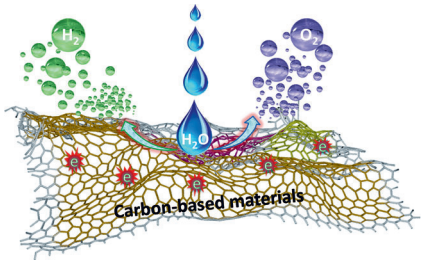

Free agents: Carbon-based metal-free catalysts have been intensively researched as alternatives to noble-metal/metal oxide catalysts for the oxygen evolution reaction (OER) in metal–air batteries and for the splitting of water through the hydrogen evolution reaction (HER). This Review gives an overview of recent developments in this area, with a focus on the OER and HER.